DETERMINING APPLICABILITY OF NOVEL MOUSE MODEL AS MODEL FOR STUDYING FOXG1 DISORDER

By

Rebekah Leigh McMahan

Thesis

Submitted to the Faculty of the

Graduate School of Vanderbilt University

in partial fulfillment of the requirements

for the degree of

MASTER OF SCIENCE

in

Neuroscience

August 9, 2019

Nashville, Tennessee

Approved:

Jeffrey L. Neul, M.D./Ph.D.

Hong Wei Dong, M.D./Ph.D.

TABLE OF CONTENTS

Page

LIST OF TABLES

LIST OF FIGURES

CHAPTER 1

INTRODUCTION

Foxg1 Disorder (OMIM # 164874), previously known as a congenital variant of Rett syndrome, is a devastating neurodevelopmental disorder that is caused by a heterozygous loss-of-function (LOF) mutation of the *FOXG1* gene on chromosome 14q12 in humans. A complete lack of *FOXG1* is embryonic-lethal (Xuan et al. 1995). FOXG1 Disorder has autistic-like features and is characterized by limited social interaction, epileptic seizures, dyskinesia, lack of independent mobility, feeding difficulties, severe developmental delay, and more. Neuroanatomical features gathered through MRI and PET imaging include corpus callosum agenesis, pachygyria, severe postnatal microcephaly, and moderate-to-severe myelination delay (Vegas et al. 2018). Additional perturbations in the expression of the protein, specifically overexpression, contribute to various forms of cancer in both the central nervous system and other tissues (Verginelli et al. 2013, Chan et al. 2009).

There is a considerable amount of information on the role of FOXG1 in the developing cortex, where it primarily functions as a transcriptional repressor of genes involved in cell cycle kinetics, axon guidance, cell fate specification, and more. More research is needed on the postnatal and postmitotic roles of FOXG1 for the purpose of treating the Disorder associated with it, as the protein is expressed into adulthood. This introduction will review the information currently known about the FOXG1 protein concerning cortical development, as well as an overview of FOXG1 Disorder.

FOXG1 gene and protein

Forkhead Box G1 (FOXG1) was discovered in rats in 1992 by Tao et al. and named Brain Factor-1 (BF-1). In 1994 the human version of the gene was characterized and named

Human Brain Factor-1 (Murphy et al. 1994). It was renamed FOXG1 by the Mouse Genome Nomenclature Committee in 1999. *FOXG1* is a single-exon gene translated into a Forkhead box (FOX) protein, which is a family of transcription factors involved in development. Transcription factors are proteins that control the rate of transcription of genes into RNA by binding to specific DNA sequences to either promote or suppress transcription (Latchman et al. 1997). Proteins in the FOX family contain a DNA-binding motif called the FOX domain, also known as a winged-helix domain (Lehmann et al. 2003). The Forkhead binding domain (FBD) of FOXG1 is along amino acids 181-275. Additional domains of FOXG1 are the Groucho-binding domain (GBD) and JARID-binding domain (JBD), two proteins that are also transcriptional repressors repressors (Roesch et al. 2008, Marcal et al 2005). See Figure 1.1 for information on specific FOXG1 interaction and phosphorylation domains.

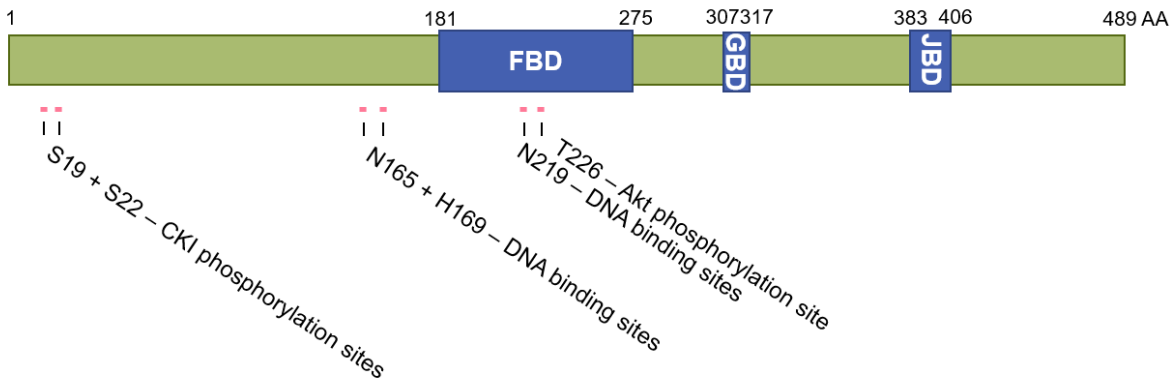

Figure 1.1. Phosphorylation and interaction domains of FOXG1 protein.

Biological functions of FOXG1

The subcellular localization of FOXG1 is an important contributor to the role FOXG1 plays. It has been found in the nucleus, cytoplasm, and the mitochondria (Regad et al. 2007, Pancrazi et al. 2015). When phosphorylated at serine 19 (S19) and S22 by casein kinase-I (CKI), FOXG1 is localized to the nucleus in neuronal progenitors and directly causes transcriptional repression (Regad et al. 2007, Li et al. 1995). Akt phosphorylation of FOXG1 at threonine 226 is shuttled into the cytoplasm, which allows neuronal progenitors to differentiate (Regad et al. 2007). In adulthood, FOXG1 can be moved back into the nucleus through being phosphorylated by CKI to suppress apoptosis (Dastidar et al. 2011). FOXG1 has also been found in the mitochondria and overexpression of FOXG1 enhanced mitochondrial membrane potential and promoted mitochondrial fission and mitosis, linking FOXG1 expression to bioenergetics important to development (Pancrazi et al. 2015).

The most important function of FOXG1 arguably is to maintain the balance of proliferation, differentiation, and apoptosis in the developing cortex. These are critically important for the proper functioning of the organism. Development of the brain is intricate and tightly controlled for this reason, with both extrinsic and intrinsic cellular cues determining patterning, proliferation, and cellular fate. Haploinsufficiency of FOXG1 leads to cells differentiating prematurely in the presence of TGF-β, an extrinsic cue that in neuronal progenitors stimulates growth arrest and cell cycle exit, triggering differentiation and thus a reduction in the progenitor pool (Dou et al. 2000, Pelton et al. 1991). The cellular interpretation of differentiation signals such as these occur in a cell-autonomous manner through the activity of different transcription factors including FOXG1 (Yang et al. 2017, Vezzali et al. 2016). However, FOXG1 does not act as a direct transcriptional repressor in the response to TGF-β but performs in a way that does not require the FBD. It instead binds to the SMAD/FOXO-protein complex, a complex involved in a wide variety of context-dependent transcription, and FOXG1 controls differentiation through repression of TGF-β/FOXO/SMAD activity (Vezzali et al.

2016, Derynck et al. 2003). A lack of FOXG1 also results in an increase in the expression of TGF-β in cultured cortical progenitors, although it has not been established whether this is through direct binding or indirect interference of expression (Vezzali et al. 2016). This serves to demonstrate that not only does FOXG1 antagonize differentiation cues in a cell-autonomous manner but also antagonizes the release of further differentiation cues from the cell.

One means by which FOXG1 prevents differentiation is through thwarting the expression of proteins involved in exiting the cell cycle, specifically p21. p21 is a cyclin-dependent kinase inhibitor downstream from TGF-β that inhibits cell-cycle progression, a trigger for differentiation in neuronal progenitors (Siegenthaler et al. 2005). In the absence of FOXG1, there is a reduction in the population in cortical intermediate progenitor cells which is in part due to increased p21 expression in proliferating zones of the developing cortex (Siegenthaler et al. 2008). Region-specific temporal regulation of cell cycle kinetics within the proliferation zones during development generates the unique structures of differentiating neocortical areas in the adult mammal (Polleux et al. 1997).

Another role of FOXG1 is in cell fate specification. This makes sense, as differentiation occurs in a specific manner with different cell types arising at different timepoints in neurodevelopment. FOXG1 affects this temporal-specific differentiation by controlling the timing of cell cycle exit and downregulating the expression of genes specific to the cell fate it suppresses (Hanashima et al. 2004, Falcone et al. 2019, Han et al. 2018). Using cultured neuronal organoids differentiated from induced pluripotent stem cells (iPSCs) derived from patients with Autism Spectrum Disorder, an overproduction of neurons of the GABAergic lineage resulted. This, and an increase in inhibitory synaptic markers and interneurons development, was found to be a result of overexpression of FOXG1 (Yang et al. 2017, Mariani et al. 2015). Surprisingly, iPSCs derived from patients with FOXG1 Disorder, and thus cells with heterozygous FOXG1 expression, were differentiated into neurons. It was found that the decrease in FOXG1 increased inhibitory synaptic markers and decreased excitatory synaptic

markers (Patriarchi et al. 2016). This shows that the role FOXG1 plays in cell fate specification is complex.

FOXG1 also antagonizes the differentiation of neuronal progenitors into Cajal-Retzius (CR) cells, interneurons, and glia in a cell-autonomous manner (Polleux et al. 1997, Brancaccio et al. 2010, Tian et al. 2012). CR cells are the earliest-born neurons that are derived from non-cortical areas, such as the cortical hem, and migrate into the cortex. CR cells are important for the guidance of migrating progenitor cells through the extracellular secretion of the guidance cue Reelin, a glycoprotein that functions in guiding newly born neurons. Guidance cues are extracellular proteins that function in axon guidance. They are either fixed in place or diffusible and function by binding to growth cones on axons and either attract or repulse axons. Reelin is attractive and in this instance attracts migrating neurons into their proper laminar identity (Chen et al. 2003). This is crucial for the proper development and specification of the cortex. FOXG1 expression must be suppressed before CR cells are differentiated (Shibata et al. 2008). In the complete absence of FOXG1, newborn progenitor cells develop the fate of CR cells with an increase in types derived in the cortical hem and pallial/subpallial boundary, resulting in an overexpression of Reelin (Siegenthaler et al. 2008, Han et al. 2018, Hanashima et al. 2002, Baek et al. 2016). This increase in CR cells is accompanied by a complete absence of cells positive for the proteins Brn2 and Ctip2, markers used to identify cortical layers 2/3 and 5/6 respectively. Upon re-expression of FOXG1 in the same system, cortical progenitors switch their competence to adopt the fate of neurons to be those normally derived from layers 5/6 (Kumamoto et al. 2013). Conversely, an overexpression of FOXG1 in the cortical hem lead to the transformation of CR cells into dentate gyrus (DG) neurons (Liu et al. 2018). This shows that FOXG1 not only suppresses cell fates but also can reprogram cells into different subtypes, further evidenced by FOXG1 being utilized to induce pluripotent stem cells and conversion of fibroblasts into GABAergic interneurons (Eiraku et al. 2008, Renner et al. 2017, Colasante et al. 2015).

Axon guidance affects not only cell migration but also forms the connections of the brain that are so vital for proper functioning of the animal. Axonal processes in FOXG1-haploinsufficient animals are randomly oriented, again due to dysregulation of guidance cues (Kumamotor et al. 2013). One important example is the involvement of FOXG1 in the formation of the corpus callosum, a thick nerve tract beneath the cerebral cortex connecting the two hemispheres of the brain and enabling communication between them. The corpus callosum is formed via guidance cues guiding the callosal axons of the callosal projection neurons, attracting them through the midline of the cortex and repulsing them from the cortical plate. FOXG1 functions in a cell-autonomous manner by coordinating with the transcription factor RP58 in callosal projection neurons to suppress the expression of key axon guidance players *Robo1* and *Slit3*, a receptor and cue that function in repulsing the callosal axons from the cortical plate (Mambetisaeva et al. 2005). FOXG1 and RP58 also suppress the expression of *Reelin* and other genes involved in migration and differentiation (Cargnin et al. 2018). Loss of only one copy of *FOXG1* results in the axons stalling at the midline and invasion of the cortical plate, contributing to the phenotype of agenesis of the corpus callosum in Foxg1 Disorder. In addition to corpus callosum formation, FOXG1 is necessary for proper thalamocortical tract patterning, a tract important for sensory input (Pratt et al. 2002).

Another contributor to axon guidance defects, found at least in interneurons, is that FOXG1 heterozygous cells have shorter and fewer axons (Yang et al. 2017). Overexpression of FOXG1 stimulates dendritic elongation and the branching of axons, causes axon overgrowth, and increases the number of GABAergic synapses (Mariani et al. 2015, Brancaccio et al. 2010, Chiola et al. 2019). The shorter axons may be from the lack of response to guidance cues. Another contributor to this could be the role of FOXG1 in mitochondria, an organelle involved in fundamental processes in neurodevelopment including the differentiation of neurons, growth of axons and dendrites, and the formation and reorganization of synapses through maintenance of bioenergetics (Gioran et al. 2014, Mattson et al. 2008).

Postnatal functions of FOXG1

The brain continues to develop even after birth. FOXG1 expression is maintained into adulthood, although its role has not been fully elucidated. A conditional deletion of FOXG1 after postnatal day 5 results in a high level of apoptosis and loss of the subgranular zone (SGZ), one of the few regions of neurogenesis maintained into adulthood (Altman et al. 1965). The SGZ generates granule cells in the hippocampus, which are believed to contribute to cognitive functions such as learning and memory (Aimone et al. 2006). Postnatally, FOXG1 is also found in the subventricular zone and the olfactory bulb, two more zones of adult neurogenesis. This suggests FOXG1 has a role in learning and memory.

FOXG1 is expressed not only in mitotic cells into adulthood but also in postmitotic neurons, which encompasses the majority of neurons in the adult brain. It has been shown to be involved in promoting survival by antagonizing cell death, demonstrated by the upregulation of FOXG1 preventing cell death in HEK293 cells primed to undergo apoptosis (Dastidar et al. 2011). Indeed, FOXG1 overexpression results in overgrowth of the cortical hem, a structure necessary to pattern the telencephalon (Ahlgren et al. 2003, Caronia-Brown et al. 2014). This appears to be mediated by a lack of normal programmed cell death as the level of apoptosis is reduced in the rostral telencephalon of mice overexpressing FOXG1, further implicating a role in antagonizing apoptosis (Martynoda et al. 2005). Apoptosis is an important occurrence in the development of the central nervous system, although the exact function it plays is not well understood. FOXG1 promotes survival through its actions as a downstream effector of the IGF-1/Akt signaling pathway, a pathway involved in the mediation of cell proliferation, apoptosis, survival, and more (Aizenman et al. 1987). As mentioned above, FOXG1 is phosphorylated by Akt for nuclear trafficking where it directly interacts with MeCP2 isoform e2 to suppress apoptosis (Dastidar et al. 2011, Dastidar et al. 2012).

FOXG1 Disorder

Patients with FOXG1 Disorder were originally diagnosed as having a variant of Rett Syndrome (RTT) (Ariani et al. 2008). RTT was observed to have three variants and once individuals were genetically sequenced, FOXG1 LOF mutations or deletions were found to be the culprit for the congenital form of RTT (Ariani et al. 2008). See Table 1.1 for a summary of the findings and prevalence of phenotypes in FOXG1 Disorder from two studies investigating genotype/phenotype correlations in FOXG1 Disorder (Vegas et al. 2018, Mitter et al. 2018).

The majority of individuals with FOXG1 Disorder possess *de novo* mutations, though one individual with a mosaic germline mutation was recorded by Mitter et al. 2018. There have been few recurrent mutations, one of which had drastically different clinical and imaging presentations (Vegas et al. 2018, Mitter et al. 2018), which illustrates that FOXG1 Disorder is not always straightforward in terms of genotype-phenotype correlations. In general, patients with N-terminal mutations and complete FOXG1 deletions show the highest global severity scores. Mitter et al. separated the mutations studied into five groups: N-terminal frameshift and nonsense (G1), N-terminal missense (G2), forkhead frameshift and nonsense (G3), forkhead missense (G4), and C-terminal frameshift and nonsense (G5). They found that G2 mutations presented with the mildest phenotype, G1 had the worst motor, speech, neurological, and neuroradiological scores, and there was a borderline significant difference between all five genotype groups concerning feeding difficulties, corpus callosum anomalies, delayed myelination, and microcephaly. There was also no significant difference in severity between G1 and G3. Individuals with missense mutations in the FBD and C-terminal domain have the lowest global severity scores (Vegas et al. 2018, Mitter et al. 2018). Six individuals carry missense mutations in a domain recently developed and expanded in primate species (Bredenkamp et al. 2007).

Of the 35 individuals that experience seizures in the study conducted by Vegas et al., generalized tonic or tonic-clonic seizures were the most frequent (Vegas et al. 2018). 17 of

Category	Phenotype	Vegas et al	Mitter et al
Motor and speech development	Unassisted sitting	NA	45%
	Unassisted walking	7%	15%
	Functional hand use	43%	40%
	Speech presence	7%	21%
Behavioral	Poor social interaction	40%	25%
	Poor eye contact	NA	52%
	Abnormal sleep patterns	64%	71%
	Unexplained crying	60%	66%
	Paroxysmal laughter		46%
Neurological features	Epilepsy	78%	68%
	Hypotonia	NA	95%
	Strabism	90%	84%
	Spasticity	NA	60%
	Stereotypic movements	79%	90%
	Dyskinesia	NA	89%
Gastrointestinal features	Feeding difficulties	71%	88%
	Gastric reflux	73%	65%
cMRI	Corpus callosum anomalies	96%	67%
	Delayed myelination	65%	56%
	Cortical anomalies	76%	72%

Table 1.1. Clinical features associated with Foxg1 Disorder.

these developed refractory epilepsy with multiple seizure types and 5 experienced at least one episode of status epilepticus. This phenotype may be due to the imbalance of glutamatergic and GABAergic cell types. An imbalance of excitatory and inhibitory signaling is common problem in individuals with ASD and individuals who experience seizures (Rubenstein et al. 2010, Casanova et al. 2003, Avoli et al. 2019). The seizure abnormalities may also be due to a dysregulation of the gene *Kcnh3*, a voltage-gated potassium channel that was found to be transcriptionally decreased in FOXG1-null cortical cultures, as deletion of this gene has caused hippocampal hyperexcitability and epilepsy in mice (Vezzali et al. 2016, Zhang et al. 2010).

There is a crucial need for therapies and treatments to address FOXG1 Disorder, as the individuals experiencing it have a markedly decreased quality of life and there are currently no identified therapies that modify the disease or address core issues such as limited mobility and social interaction deficits. Development of these therapies will prove to be difficult as FOXG1 Disorder is not diagnosed until the affected individual is born, after most of the observed structural abnormalities found in the brain have occurred. However, the postnatal and postmitotic roles of FOXG1 hold potential promise that therapies could be developed to improve clinical features even after birth. Recent works on mouse models of other neurodevelopmental disorders, such as RTT, have demonstrated the possibility of a reversal of disease via post-symptomatic re-expression or downregulation of MeCP2, the gene disrupted in RTT and overexpressed in MeCP2 Duplication Syndrome respectively (Guy et al. 2007, Sztainberg et al. 2016). A fundamental question is whether similar post-symptomatic expression of FOXG1 would be sufficient to modify or reverse symptoms in the Disorder. Although FOXG1 Disorder currently has no approved therapies, a triheptanoin-based diet has been used to treat FOXG1 heterozygous mice and was shown to rescue hippocampal hyperexcitability and seizure susceptibility (Testa et al. 2019). This gives us hope that other core characteristics of FOXG1 can be remediated, even when administered after symptom onset.

Summary

The protein FOXG1 is an ancient transcription factor necessary for the proper formation of the cortex in all vertebrate animals. It has an impact on cellular proliferation, differentiation, cellular migration, and more factors involved in cortical development. FOXG1 Disorder is not diagnosed until after the birth of the individual, making it critical to develop therapies to address the Disorder postnatally. The laboratory of Dr. Jeffrey Neul developed a novel mouse line expressing one functional copy of the FOXG1 gene and could later in theory be induced to express two copies. The aim of my project was first to determine the applicability of this mouse line studying FOXG1 Disorder through the ability of the mouse line to recapitulate the molecular, structural, and behavioral phenotypes of the Disorder. The second part of my project was to induce the expression of both copies of FOXG1 at specific developmental timepoints in order to determine the potential of postnatal phenotypic rescue, as well as to determine the time points at which FOXG1 reinstatement is necessary to address specific phenotypes.

CHAPTER 2

CHARACTERIZING THE NEUROBEHAVIORAL, STRUCTURAL, AND MOLECULAR ALTERATIONS IN FOXG1- KI MOUSE LINE

Introduction

FOXG1 Disorder is a devastating neurodevelopmental disorder caused by a loss-of-function (LOF) mutation of the *FOXG1* gene that affects females as equally as males (Vegas et al. 2018). For the purpose of studying FOXG1 Disorder, we have recently developed a FOXG1 heterozygous knock-out/knock-in (FOXG1-KI) mouse model. This novel mouse line carries one functional wild-type copy of the *FOXG1* gene (Figure 2.1.a) as well as a floxed stop cassette before another *FOXG1* gene fused with an HA tag (Figure 2.1.b). Mice subsequently express only one copy of the *FOXG1* gene and are called KI. These mice are meant to model individuals with FOXG1 Disorder that carry only one working copy of the *FOXG1* gene, while providing the opportunity to conditionally express (via Cre-driven recombination removal of the stop cassette) wild-type levels of *FOXG1* to determine the ability to rescue phenotypes by restoring *FOXG1* expression. The initial step of this project was to investigate the applicability of this model to model the FOXG1 Disorder. Thus, I performed behavioral, structural, and molecular assays to identify phenotypic abnormalities in this mouse model. My work provides evidence that this mouse model is applicable to recapitulate phenotypes associated with FOXG1 Disorder

Molecular phenotypes

To validate that there are differences in the levels of the FOXG1 protein in KI mice, I ran a western blot using hemibrain lysates isolated from three KI animals as well as three WT animals. I found that KI animals had 70% of the level of FOXG1 protein compared to WT animals (Figure 2.2).

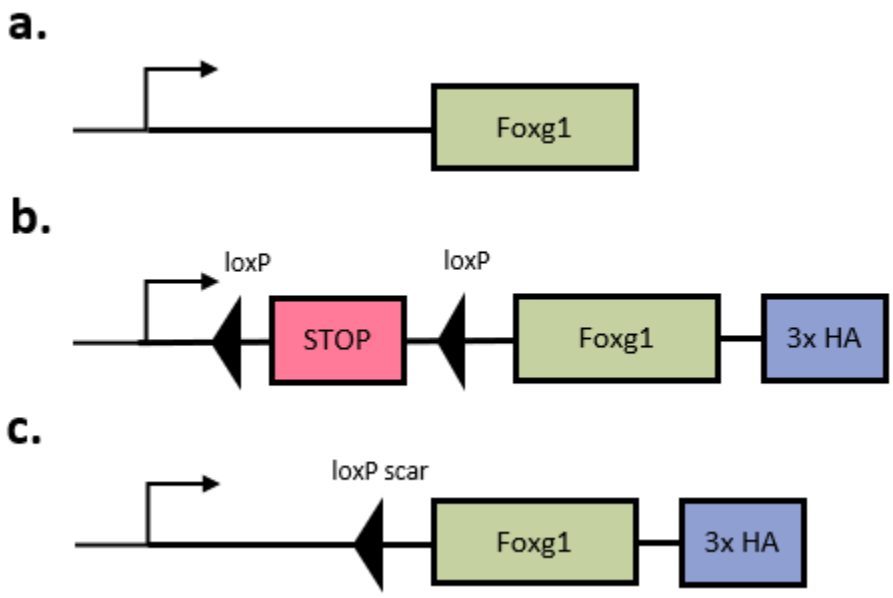

Figure 2.1. Genetic schematic of FOXG1-KI mouse line. **a**. Wild type copy of *FOXG1* gene. **b**. Copy of *FOXG1* gene preceded by a stop cassette and fused to an HA tag. **c**. Copy of *FOXG1-HA* gene.

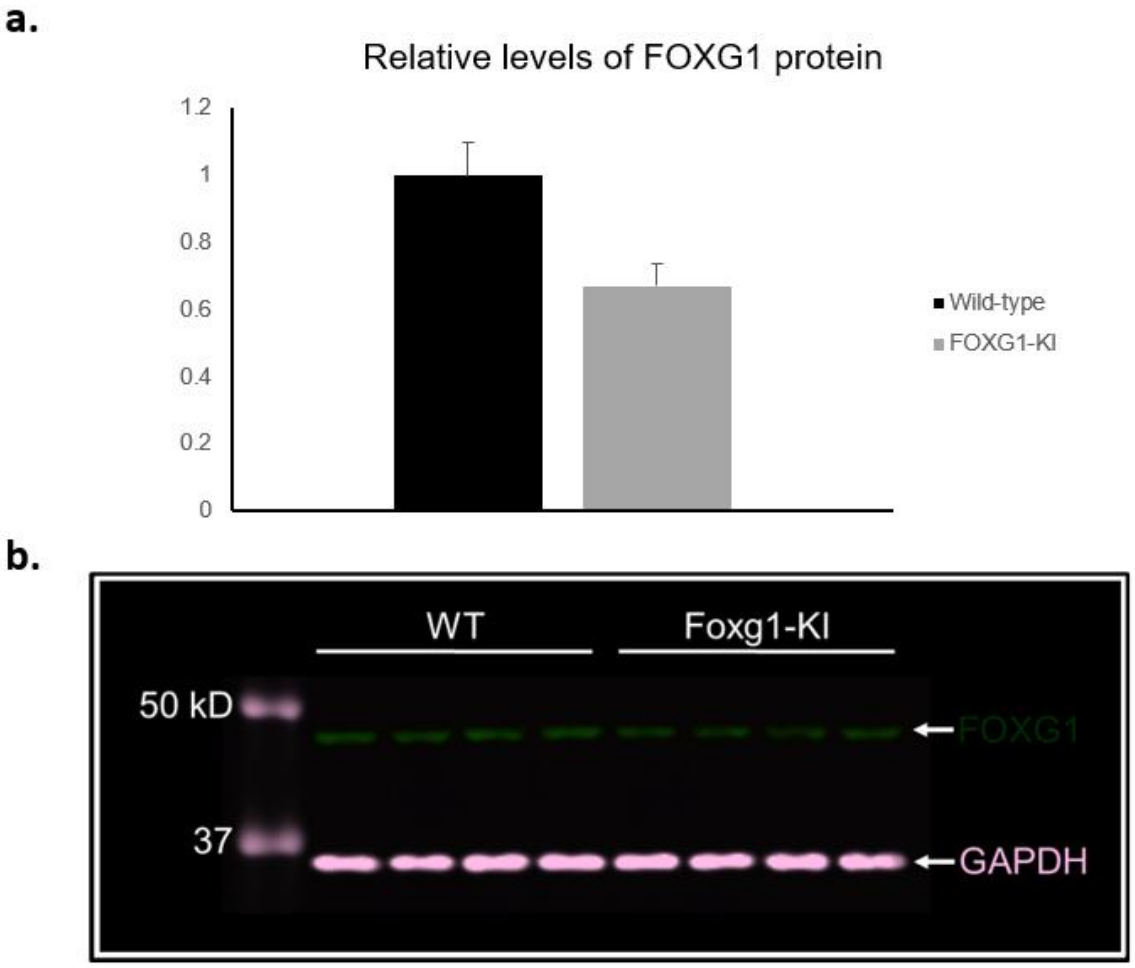

Figure 2.2. Western blot for protein quantification of FOXG1 in wild-type animals compared to KI animals. **a**. Quantification levels of FOXG1 protein. **b**. Image of western blot

Structural phenotypes

To determine cellular and structural abnormalities due to insufficient dosage of FOXG1 protein I performed immunohistochemistry (IHC). The most success I had with IHC is when I performed an antigen retrieval protocol followed by exposure to rabbit anti-FOXG1 antibody 1:500. See Figure 2.3, which is a sagittal view of the hippocampus of mice viewed on an Olympus BX51 microscope at 10X magnification. The image is taken with an iPhone camera through the lens. Previous work has found structural abnormalities in the hippocampus of mice lacking one copy of *FOXG1* (Tian 2012), so I initially focused attention on this brain region. The cell body-rich regions of the hippocampus are not as tightly grouped in the KI animal compared to WT animals. The hippocampus is malformed and there is no distinct beginning or end of the dentate gyrus (DG). The formation of both the suprapyramidal and infrapyramidal blades of the DG was severely disrupted.

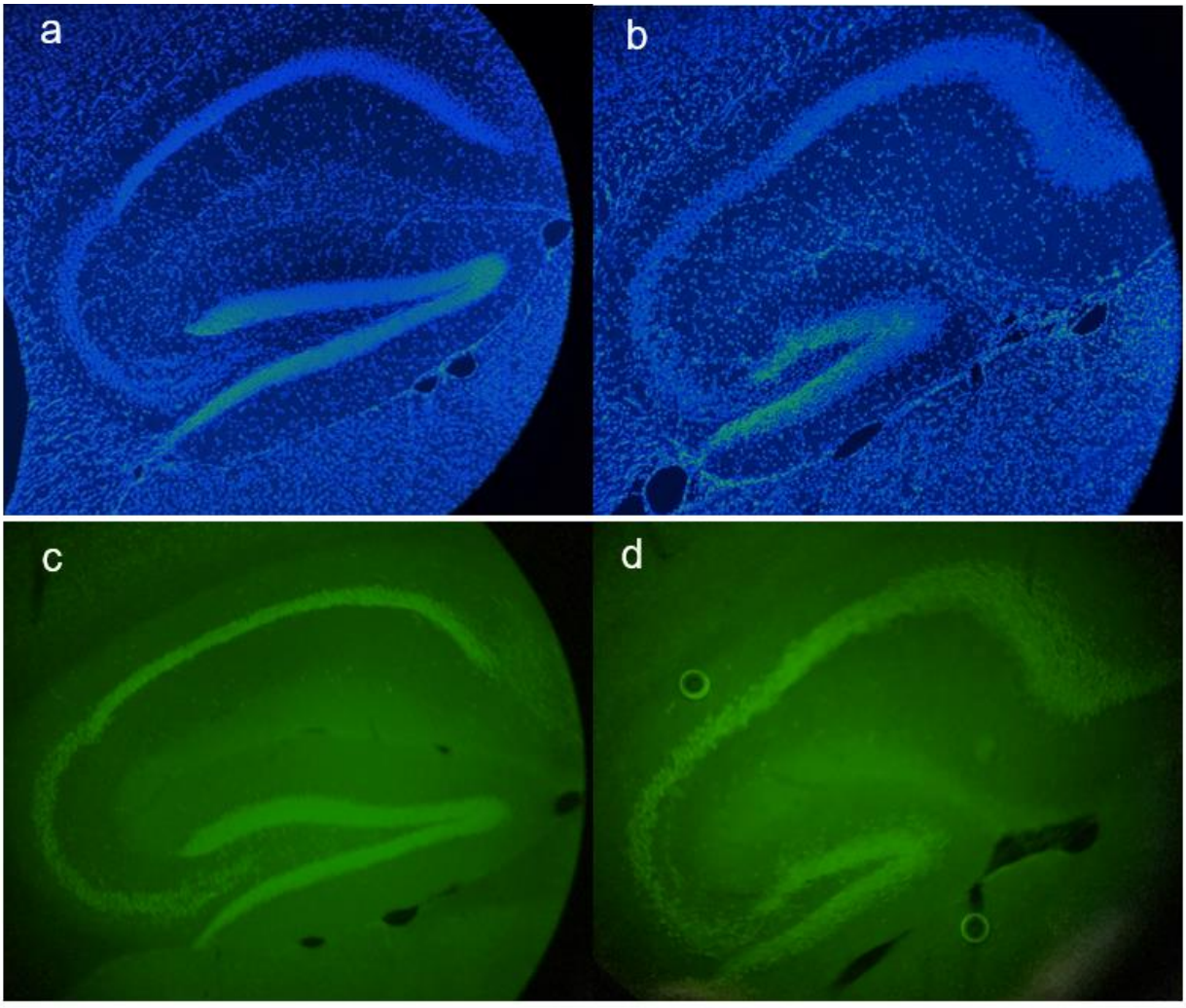

Figure 2.3. Immunohistochemistry image. **a**. DAPI exposure of wild-type hippocampus. **b**. DAPI exposure of KI hippocampus. **c**. FOXG1 protein probe of wild-type hippocampus. **d**. FOXG1 protein probe of KI hippocampus.

To further determine structural phenotype associated with our FOXG1-KI model, diffusion tensor imaging (DTI) was performed using six WT and six KI brains. The parameters bound pool fraction (BPF) (Figure 2.4.a), apparent diffusion coefficient (ADC) (Figure 2.4.b), and the fractional anisotropy (FA) (Figure 2.4.c) of the corpus callosum, thalamus, and hippocampus as well as the volume of the hippocampus and corpus callosum (Figure 2.4.d) were evaluated by collaborators the Does Lab. ADC is a measure of the magnitude of the diffusion of water molecules within tissue. See Table 2.1 for the averages of all parameters. BPF estimates the proportion of exchanging protons bound to macromolecules, such as those found in myelin, and is a direct measure of myelin content. The FA describes the degree of anisotropy of a diffusion process. The results showed a significant difference between the WT and KI animals for the BPF, volume, and ADC of the corpus callosum, and the ADC and FA of the hippocampus.

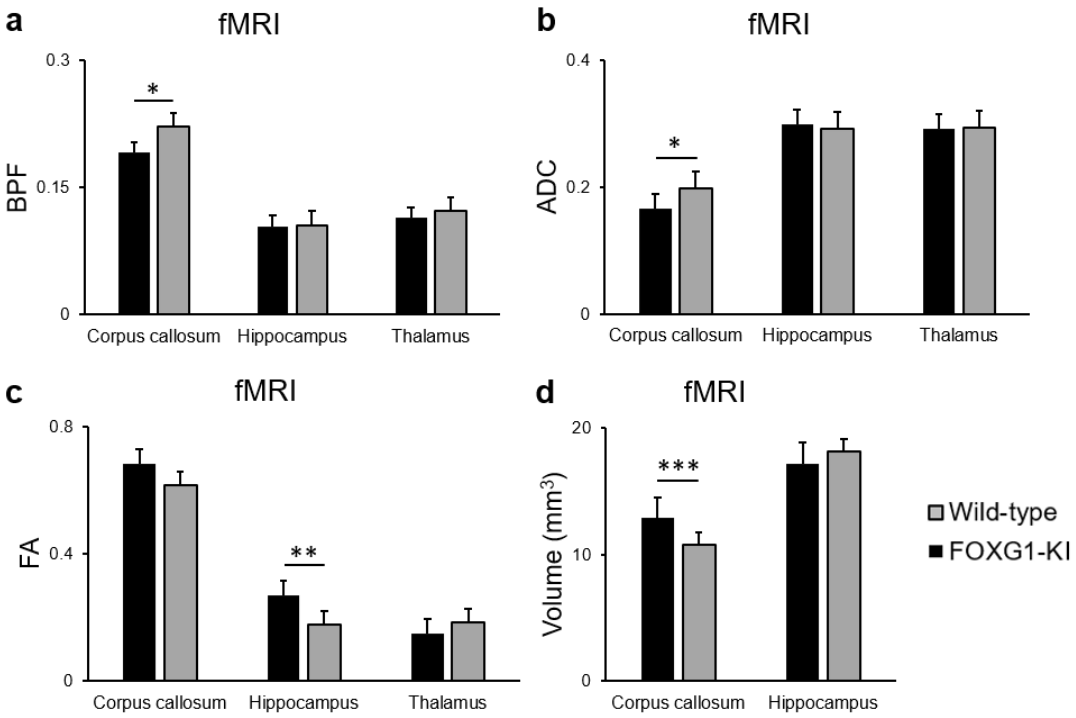

Figure 2.4. Diffusion tensor imaging of FOXG1-KI compared to wild-type mice. **a**. Bound pool fraction (BPF) of the corpus callosum, hippocampus, and thalamus **b**. Apparent diffusion coefficient (ADC) of the corpus callosum, hippocamps, and thalamus. **c**. Fractional anisotropy (FA) of the corpus callosum, hippocamps, and thalamus. **d**. Volume of the corpus callosum and hippocampus. (* $p < 0.05$, ** $p < 0.01$, *** $p < 0.001$)

		Wild-type average	FOXG1-KI average
BPF	Corpus callosum	0.191 ± 0.01	0.222 ± 0.02
	Hippocampus	0.104 ± 0.02	0.105 ± 0.01
	Thalamus	0.114 ± 0.01	0.122 ± 0.02
ADC	Corpus callosum	0.165 ± 0.02	0.198 ± 0.03
	Hippocampus	0.299 ± 0.03	0.292 ± 0.02
	Thalamus	0.291 ± 0.02	0.294 ± 0.03
FA	Corpus callosum	0.683 ± 0.08	0.618 ± 0.06
	Hippocampus	0.269 ± 0.04	0.178 ± 0.04
	Thalamus	0.149 ± 0.02	0.184 ± 0.03
Volume (mm^3)	Corpus callosum	12.85 ± 0.9	10.73 ± 0.6
	Hippocampus	17.18 ± 1.5	18.16 ± 1.4

Table 2.1. Diffusion tensor imaging of FOXG1-KI compared to wild-type mice.

Behavioral phenotypes

To determine the presence of applicable behavioral phenotypes in our FOXG1-KI mouse model, I performed behavioral assays in the Vanderbilt University Neurobehavior Core to detect changes in activity levels, anxiety, motor learning, object memory, sociability and social novelty seeking, aggression, and gait dysfunction. Figure 2.5 shows the timeline of the behavioral assays. Following conducting the behavioral assays, I ran a general linear model using the factors of genotype and sex that showed there was a significant difference between sexes in various tests so in our data analyses we compared male WT (five animals) to male KI (eight animals), and female WT (seven animals) to female KI (seven animals).

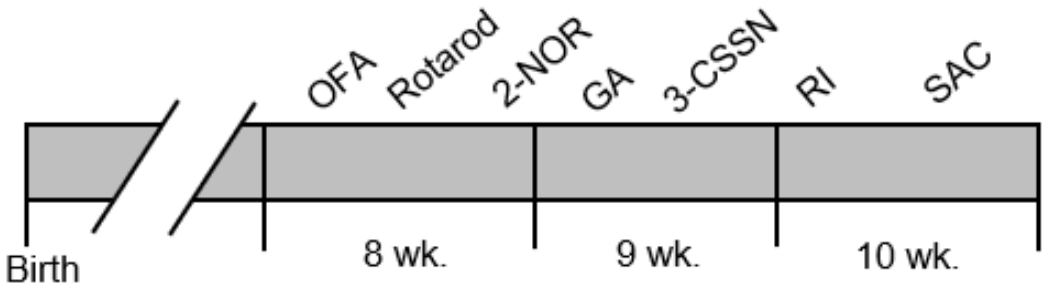

Figure 2.5. The timeline of the behavioral assays performed with the FOXG1-KI mice. OFA = open field analysis, 2-NOR = 2-Novel object recognition, GA = gait analysis, 3-CSSN = 3-chamber sociality and social novelty, RI = resident intruder, SAC = sacrifice.

Behavioral phenotypes: open field analysis

To determine the presence of changes of activity levels of our FOXG1-KI mice, I used the behavioral assay open field analysis (OFA) for the span of one hour. This test measured the parameters of ambulatory distance, vertical count, and duration. I drew a grid that separated the detection of parameters into the center of the field and at the edge of the field. Thus, this test also has implications for anxiety phenotypes as subjects experiencing more anxiety will spend less time in open spaces. Table 2.2 contains the summation of OFA data. I detected significant changes between WT and KI males for total ambulatory distance (Figure 2.6.a), ambulatory distance in the center (Figure 2.6.b), the fraction of total distance traveled in the center (Figure 2.6.c), the fraction of total duration spent in the center (Figure 2.6.d), and the fraction of vertical beam breaks in the center (Figure 2.7.c). I detected significant changes between WT and KI females for total ambulatory distance (Figure 2.6.a), ambulatory distance in the center of the field (Figure 2.6.b), the fraction of total distance moved in the center of the field (Figure 2.6.c), the fraction of the duration of time spent in the center of the field, (Figure 2.6.d), total vertical count (Figure 2.7.a), and the vertical count in the center of the field (Figure 2.7.b), and the fraction of vertical beam breaks in the center (Figure 2.7.c). This leads us to conclude that KI mice as a whole are hypoactive and have increased anxiety.

		Male			Female		
Test	Parameter	Wild-type average	FOXG1-KI average	p value	Wild-type average	FOXG1-KI average	p value
OFA	Ambulatory distance center (cm)	5590 ± 480	2770 ± 327	0.00015	5010 ± 706	1990 ± 115	0.0012
	Ambulatory distance edge (cm)	3700 ± 382	3770 ± 465	0.87	3450 ± 400	2910 ± 110	0.22
	Total ambulatory distance (cm)	9500 ± 420	6410 ± 814	0.033	8450 ± 998	4900 ± 123	0.0041
	Vertical count center (#)	242 ± 36	122 ± 28	0.16	333 ± 69	87.6 ± 15	0.0045
	Vertical count edge (#)	340 ± 36	381 ± 37	0.27	387 ± 51	275 ± 21	0.067
	Total vertical count (#)	581 ± 39	503 ± 58	0.96	720 ± 103	362 ± 33	0.0063
	Duration in center (s)	1650 ± 130	1330 ± 223	0.33	1880 ± 153	1200 ± 122	0.0049
	Fraction of duration in center	0.457 ± 0.036	0.371 ± 0.043	0.046	0.521 ± 0.043	0.334 ± 0.034	0.0049
	Fraction of distance in center	0.45 ± 0.035	0.37 ± 0.019	0.00075	0.52 ± 0.028	0.33 ± 0.019	0.00018
	Fraction of vertical count in center	0.418 ± 0.030	0.236 ± 0.031	0.0021	0.441 ± 0.050	0.236 ± 0.027	0.0038

Table 2.2. Table containing the averages, SEM, and p values of parameters for the behavioral test open field analysis (OFA). p values were calculated using a two-tailed t-test. Significant p values are highlighted in yellow.

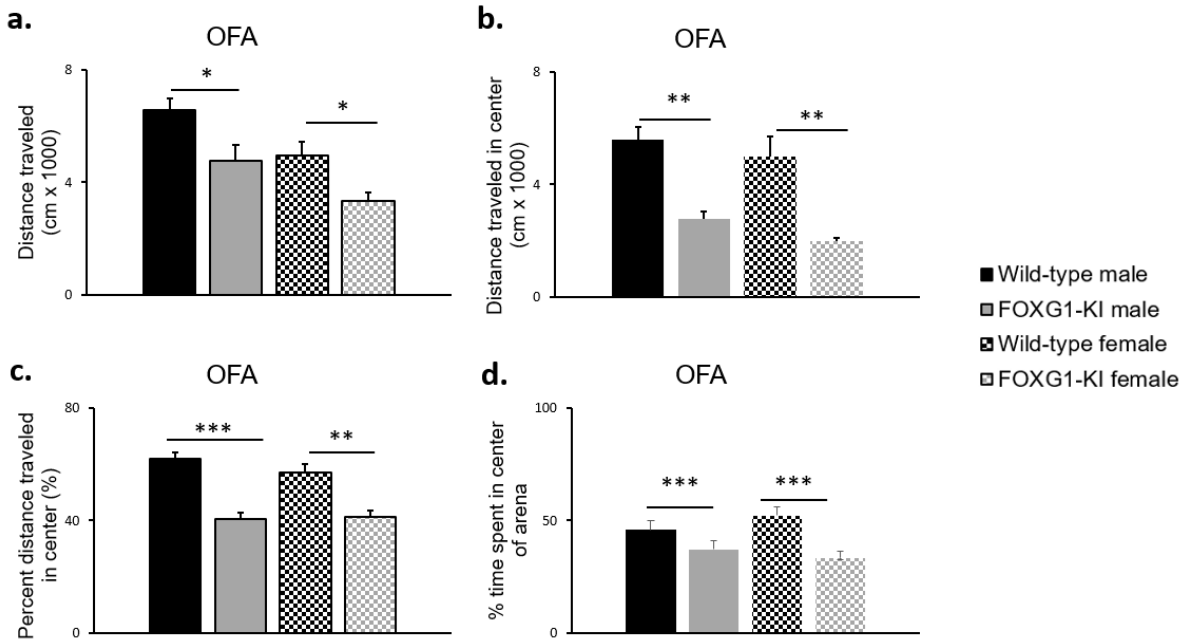

Figure 2.6. Graphs of time and distance parameters of open field analysis (OFA). **a**. Total ambulatory distance traveled. **b**. Ambulatory distance traveled in the center of the arena. **c**. The fraction of total distance traveled that was traveled in the center of the arena. **d**. The fraction of the total duration of time spent in the center of the arena. (* $p < 0.05$, ** $p < 0.01$, *** $p < 0.001$)

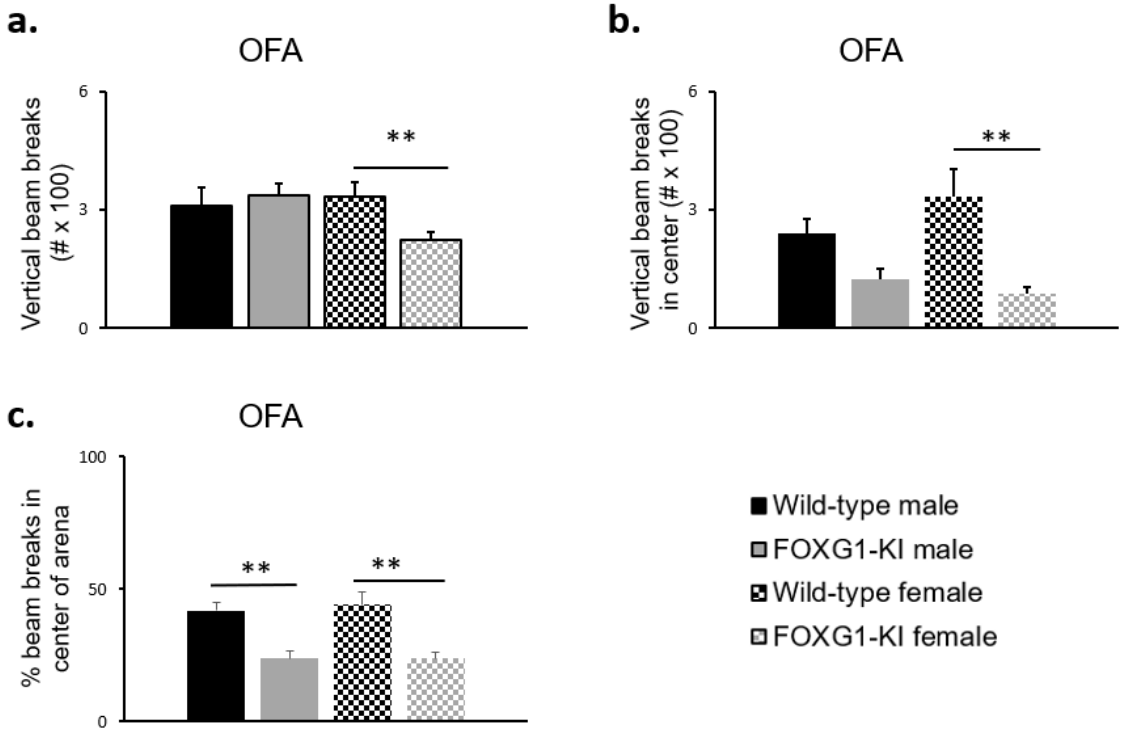

Figure 2.7. Graphs of vertical beam breaks during open field analysis (OFA). **a**. Total number of vertical beam breaks. **b**. Vertical beam breaks in the center of the arena. **c**. The fraction of total beam breaks that was performed in the center of the arena. (* $p < 0.05$, ** $p < 0.01$, *** $p < 0.001$)

Behavioral phenotypes: accelerating rotarod

To detect changes in motor learning, I conducted the accelerating rotarod behavioral assay. Table 2.3 contains the summation of data for rotarod. I detected no significant differences between WT and KI male mice for any of the three days. I detected significant differences between WT and KI female mice for day two and day three of Rotarod testing, and no significant difference for day one (Figure 2.8). This leads me to conclude that female KI mice have a deficit in motor learning.

		Male			Female		
Test	Parameter	Wild-type average	FOXG1-KI average	p value	Wild-type average	FOXG1-KI average	p value
Rotarod	Latency to fall Day 1 (s)	223 ± 12	222 ± 13	0.95	257 ± 18	213 ± 13	0.068
	Latency to fall Day 2 (s)	205 ± 19	209 ± 14	0.85	259 ± 14	195 ± 19	0.021
	Latency to fall Day 3 (s)	208 ± 37	210 ± 16	0.94	255 ± 23	177 ± 19	0.022

Table 2.3. Table containing the averages and SEM of parameters for the behavioral test accelerating rotarod. p values were calculated using a two-tailed t-test. Significant p values are highlighted in yellow.

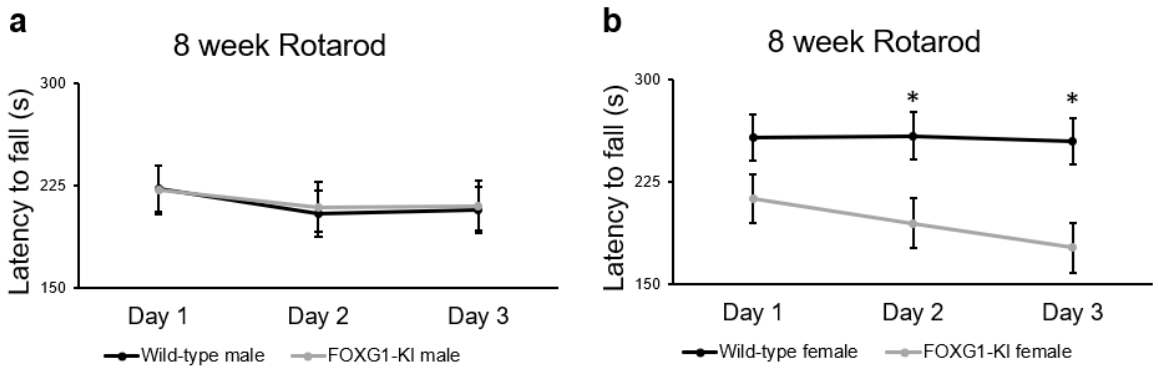

Figure 2.8. Graphs of rotarod test. **a**. Male rotarod **b**. Female rotarod. (* $p < 0.05$, ** $p < 0.01$, *** $p < 0.001$)

Behavioral phenotypes: novel object recognition

To detect changes in object memory, I conducted the Novel Object Recognition (NOR) task. I recorded the parameters of time spent investigating the novel object, number of approaches to the novel object, time spent investigating the familiar object, and the number of approaches to the familiar object. To quantify the presence of changes in memory, I calculated the difference in time spent investigating the novel and familiar object as well as the discrimination index (DI) of the time spent investigating each object. The DI is the amount of time spent with the novel object subtracted by the amount of time spent with the familiar object, divided by the total amount of time spent investigating objects [DI = (time NO – time FO) / total time]. Table 2.4 contains the summation of data for NOR. I detected no significant changes between WT and KI males for any parameter. I detected significant changes between WT and KI females for time difference (Figure 2.9.a) and total time spent investigating objects (Figure 2.9.b). It is difficult to interpret this because there is a significant difference in total time spent investigating for females (Figure 2.9.c), which suggests that the difference in time spent investigating the objects is due to that aspect and not anything to do with memory changes. There is a trend for the KI animals, both male and female, to overall spend more time investigating the novel object than the familiar.

		Male			Female		
Test	Parameter	Wild-type average	FOXG1-KI average	p value	Wild-type average	FOXG1-KI average	p value
NOR	Time spent novel (s)	33.3 ± 5.8	50.4 ± 10	0.23	33.6 ± 2.1	61.4 ± 12	0.025
	Time spent familiar (s)	18.0 ± 1.7	21.8 ± 4.8	0.56	28.0 ± 4.6	29.2 ± 3.0	0.84
	Approaches novel	25.0 ± 1.6	24.5 ± 2.0	0.87	27.4 ± 1.7	28.1 ± 1.5	0.98
	Approaches familiar	15.8 ± 1.7	15.3 ± 2.2	0.86	20.6 ± 2.8	19.0 ± 1.6	0.22
	Time difference (s)	15.3 ± 4.3	28.6 ± 10.7	0.37	32.2 ± 12	5.67 ± 5.7	0.032
	DI time	0.276 ± 0.045	0.366 ± 0.085	0.45	0.122 ± 0.095	0.304 ± 0.080	0.059
	Total time investigating (s)	51.2 ± 7.3	72.2 ± 11.4	0.21	61.6 ± 4.2	90.6 ± 13	0.043

Table 2.4. Table containing the averages and SEM of parameters for the behavioral test novel object recognition (NOR). p values were calculated using a two-tailed t-test. Significant p values are highlighted in yellow.

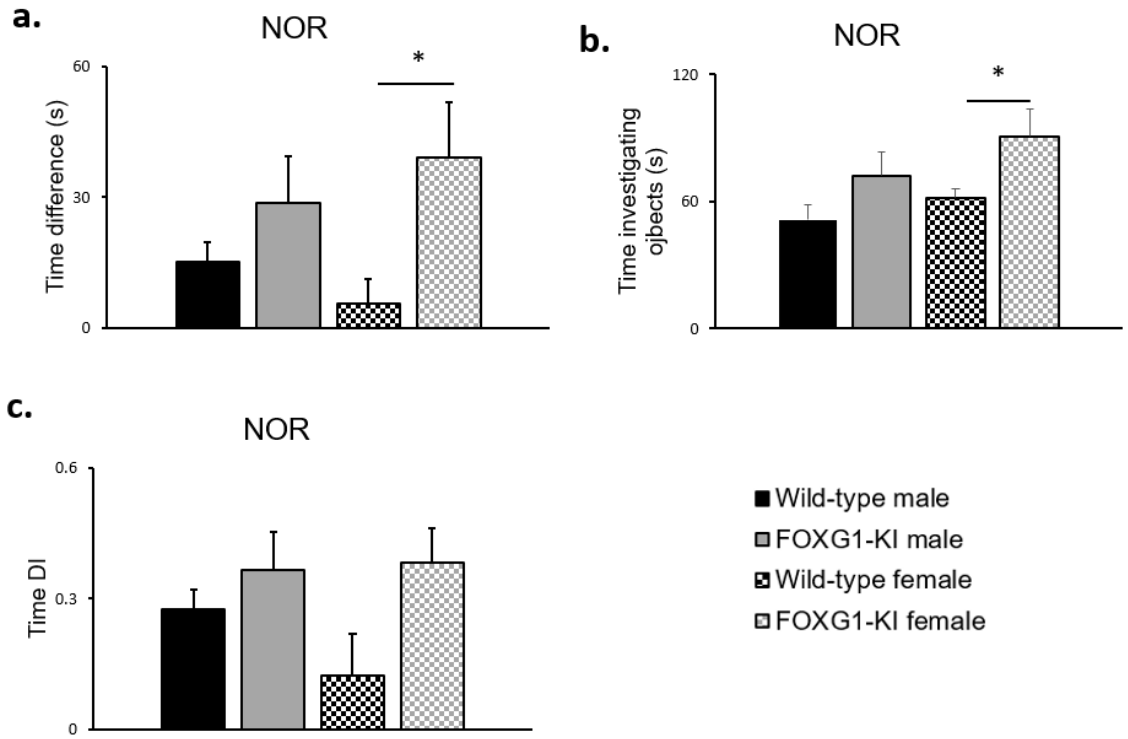

Figure 2.9. Graphs of novel object recognition (NOR) parameters. **a**. The difference in time for investigating novel object (NO) compared to familiar object (FO), (NO time – FO time). **b**. Total time spent investigating objects. **c**. The discrimination index for time spent investigating the NO, [(NO time – FO time) / (NO time + FO time)] (* $p < 0.05$, ** $p < 0.01$, *** $p < 0.001$)

Behavioral phenotypes: 3-chamber sociability and social novelty

To detect changes in sociability and social novelty seeking, I used the behavioral paradigm 3-chamber sociability and social novelty (3-CSSN) test. This test takes place in a box with three chambers (Figure 2.10) with two rounds. In the first round, there is one pencil cup containing a mouse (S1) and one empty cup (Emp). In the second round, the S1 cup remains and a second mouse (S2) is placed in the cup previously empty. I drew a grid for the ANY-maze software to identify the location of the mouse in relation to the chambers. The different locations are thus: S1 chamber, S1 cup, center chamber, Emp/S2 chamber, Emp/S2 cup. The software recorded distance traveled, entries into each area, and the time spent in each area. I also calculated Sociability Index (SI) using Round 1 data as well as Social Novelty Index (SNI) using Round 2 data. Sociability is defined as the quality of being social and is demonstrated by the animal seeking out other animals to be near (S1) rather than to be alone (Emp). Preference for social novelty is demonstrated by the animal investigating a novel mouse (S2) rather than interacting with a previously-known mouse (S1). Table 2.5 contains the summation of the averages for the parameters recorded in 3-CSSN.

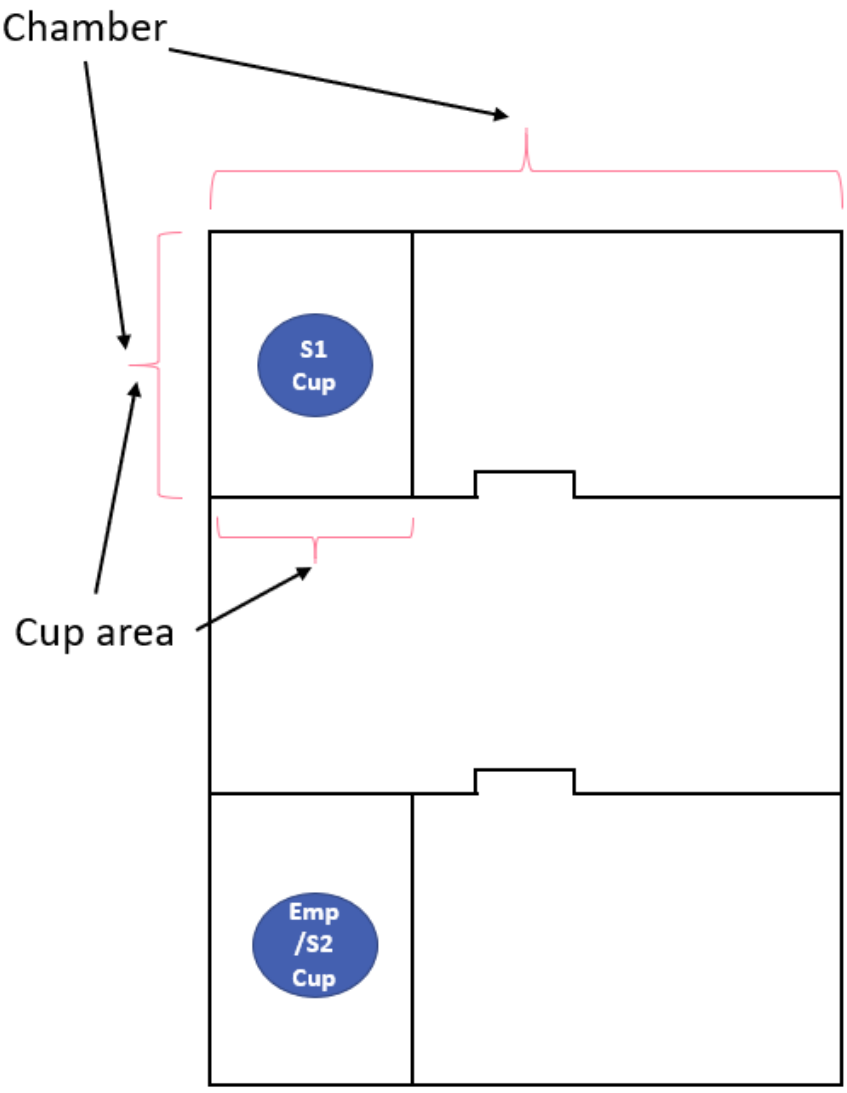

Figure 2.10. Layout of the chamber used for the 3-chamber sociability and social novelty test.

		Male			Female		
Test	Parameter	Wild-type average	FOXG1-KI average	p value	Wild-type average	FOXG1-KI average	p value
	Distance traveled round 1 (m)	30.1 ± 1.8	24.9 ± 1.3	0.0397	31.9 ± 1.5	26.5 ± 1.0	0.012
	Distance traveled round 2 (m)	25.7 ± 1.8	20.9 ± 1.6	0.077	23.7 ± 1.4	21.3 ± 0.69	0.14
	Total distance traveled (m)	55.8 ± 3.1	45.8 ± 2.7	0.036	55.7 ± 2.7	47.8 ± 1.3	0.023
	Round 1: Time spent in S1 chamber (s)	249 ± 7.1	324 ± 21	0.022	262 ± 15	303 ± 22	0.16
	Round 1: Entries into S1 chamber (#)	18.4 ± 2.0	9.6 ± 0.94	0.00086	20.9 ± 1.7	12.9 ± 1.7	0.0055
	Round 1: Time spent in S1 cup area (s)	143 ± 15.6	209 ± 25	0.087	159 ± 14	219 ± 15	0.011
	Round 1: Entries into S1 cup area (#)	20.2 ± 1.5	26.8 ± 2.9	0.12	23.3 ± 2.2	30.6 ± 1.6	0.019
	Round 1: Time spent in empty chamber (s)	239 ± 10	198 ± 17	0.10	218 ± 14	193 ± 14	0.24
	Round 1: Entries into empty chamber (#)	19.2 ± 2.7	7.8 ± 0.37	0.00023	19.6 ± 1.3	9.43 ± 0.72	1.71159E-05
	Round 1: Time spent in empty cup area (s)	137 ± 4.6	116 ± 16	0.32	123 ± 13	119 ± 13	0.83
	Round 1: Entries into empty cup area (#)	20.8 ± 1.7	19.5 ± 3.3	0.77	22.7 ± 2.2	17.9 ± 1.4	0.088
	Round 1: Time spent in center chamber (s)	112 ± 9.6	78.9 ± 6.9	0.015	119 ± 8.1	104 ± 11	0.27
	Round 1: Entries into center chamber (#)	36.8 ± 4.6	16.5 ± 1.1	0.00025	38.9 ± 2.7	21.6 ± 1.8	0.00018
3-CSSN	Round 1: Sociablity index chamber	0.0229 ± 0.031	0.238 ± 0.070	0.042	0.0935 ± 0.059	0.217 ± 0.066	0.19
	Round 1: Sociability index cup	0.0112 ± 0.041	0.265 ± 0.10	0.095	0.129 ± 0.063	0.294 ± 0.071	0.11
	Round 2: Time spent in S1 chamber (s)	172 ± 22	236 ± 35	0.20	164 ± 8.7	195 ± 17	0.13
	Round 2: Entries into S1 chamber (#)	15.8 ± 1.7	9.60 ± 1.4	0.017	13.9 ± 1.4	9.71 ± 0.36	0.015
	Round 2: Time spent in S1 cup area (s)	83.7 ± 20	156 ± 38	0.18	100 ± 9.3	135 ± 17	0.10
	Round 2: Entries into S1 cup area (#)	13.6 ± 3.7	16.9 ± 2.5	0.47	14.0 ± 1.2	16.4 ± 1.0	0.14
	Round 2: Time spent in S2 chamber (s)	305 ± 21	265 ± 21	0.22	178 ± 20	189 ± 21	0.21
	Round 2: Entries into S2 chamber (#)	17.4 ± 1.8	9.90 ± 1.2	0.0038	21.6 ± 2.5	22.0 ± 1.6	0.89
	Round 2: Time spent in S2 cup area (s)	166 ± 14	150 ± 15	0.47	178 ± 20	189 ± 21	0.72
	Round 2: Entries into S2 cup area (#)	24.8 ± 2.0	23.6 ± 3.4	0.8	21.6 ± 2.5	22.0 ± 1.6	0.89
	Round 2: Time spent in center chamber (s)	124 ± 13	98.9 ± 16	0.3	107 ± 8.8	105 ± 11	0.88
	Round 2: Entries into center chamber (#)	30.4 ± 4.0	16.1 ± 2.2	0.0059	28.3 ± 2.8	14.3 ± 1.1	0.00052
	Round 2: Social novelty index chamber	0.281 ± 0.085	0.0781 ± 0.11	0.21	0.333 ± 0.035	0.215 ± 0.069	0.15
	Round 2: Social novelty index cup	0.346 ± 0.13	0.0549 ± 0.15	0.21	0.273 ± 0.045	0.168 ± 0.010	0.35

Table 2.5. Table containing the averages and SEM of parameters for the behavioral test 3-chamber sociability and social novelty (3-CSSN). p values were calculated using a two-tailed t-test. Significant p values are highlighted in yellow. S1 = Stranger 1, S2 = Stranger 2.

For the males in Round 1, I detected significant differences in entries into S1 chamber (Figure 2.11.a), entries into Emp chamber (Figure 2.11.b), entries into center chamber (Figure 2.11.c), time spent in Stranger 1 chamber (Figure 2.12.a), time spent in center chamber (Figure 2.12.c), and SI for the chambers (Figure 2.13.a). For the females in Round 1, I detected significant differences in entries into S1 chamber (Figure 2.11.b), entries into Emp chamber (Figure 2.11.b), entries into center chamber (Figure 2.11.c), entries into S1 cup area (Figure 2.11.d), and time spent in S1 cup area (Figure 2.12.d).

For the males in Round 2, I detected significant differences in entries into S1 chamber (Figure 2.14.a), entries into S2 chamber (Figure 2.14.b), and entries into the center chamber (Figure 2.14.c). There were no significant differences for any time parameters for Round 2 (Figure 2.15). For the females in Round 2, I detected significant differences for entries into S1 chamber (Figure 2.14.a), entries into S2 chamber (Figure 2.14.b), and entries into the center chamber (Figure 2.14.c). There were no significant differences for any time parameters for Round 2 (Figure 2.15).

In addition to these parameters, I found a significant difference in distance traveled in Round 1 (Figure 2.16.a) as well as total distance traveled (Figure 2.16.c) for both male and female KI mice. The difference in entries in Round 1 can most likely be accounted for by the difference in distance traveled. However, in Round 2 there is no significant difference in distance traveled so the entries may not be accounted for by that. Overall, there is a trend for KI animals to have higher SI scores than WT animals and lower SNI scores than WT animals.

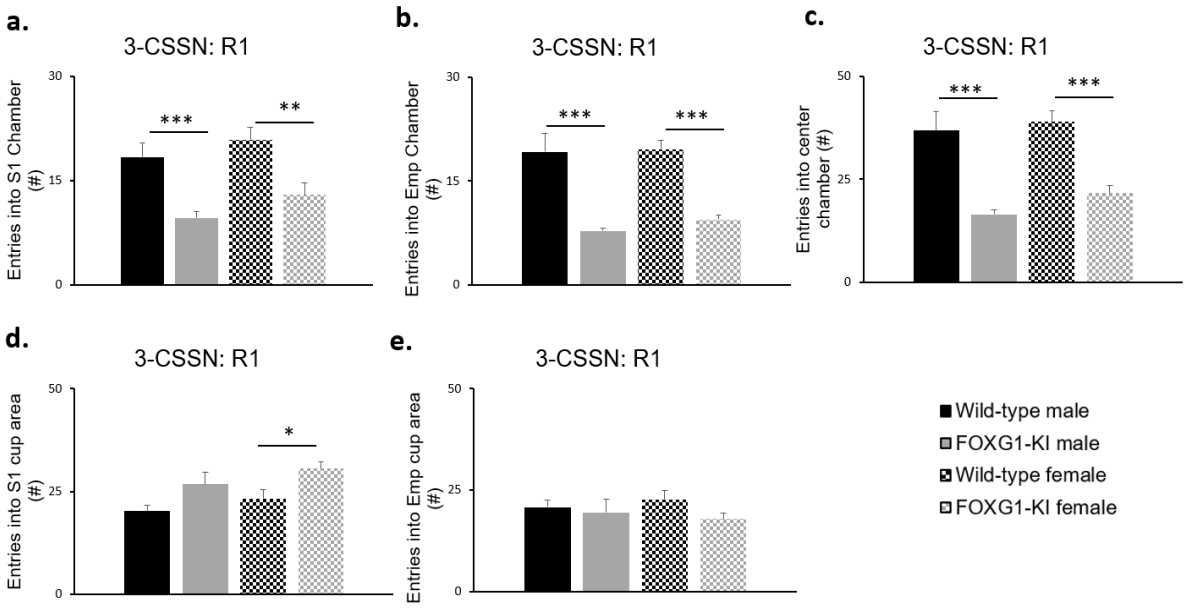

Figure 2.11. Graphs for location entries in 3-chamber sociability and social novelty (3-CSSN) test round 1 (R1). **a**. Entries into stranger 1 (S1) chamber. **b**. Entries into empty chamber. **c**. Entries into center chamber. **d**. Entries into S1 cup area. **e**. Entries into empty cup area (* $p < 0.05$, ** $p < 0.01$, *** $p < 0.001$)

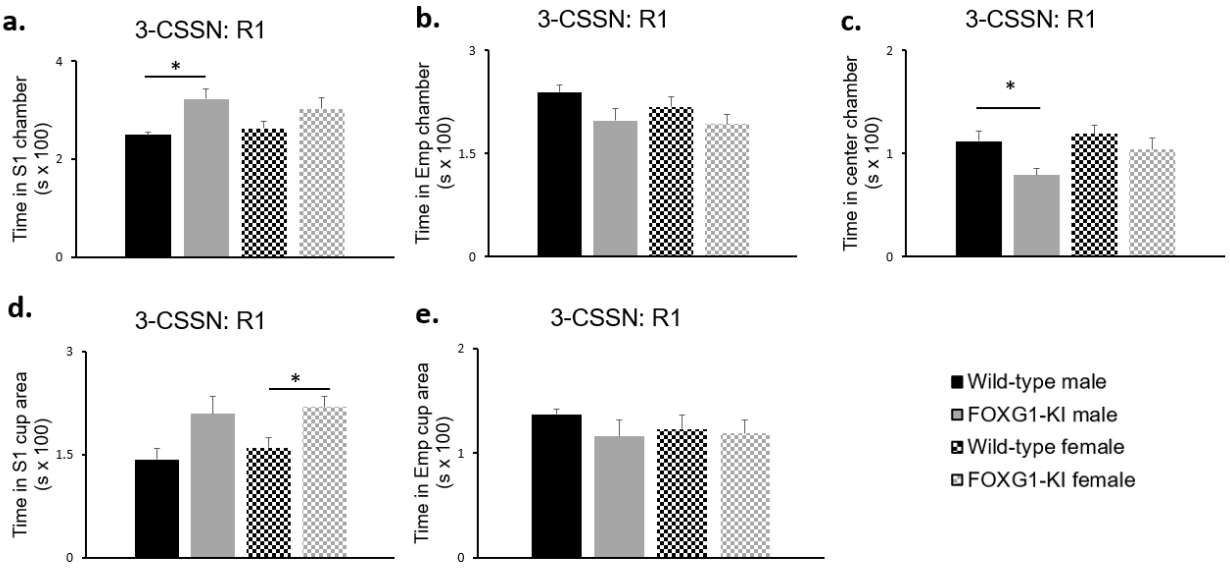

Figure 2.12. Graphs of durations in 3-chamber sociability and social novelty (3-CSSN) test round 1 (R1). **a**. Time in S1 chamber. **b**. Time in empty chamber. **c**. Time in center chamber. **d**. Time in S1 cup area. **e**. Time in empty cup area. (* $p < 0.05$, ** $p < 0.01$, *** $p < 0.001$)

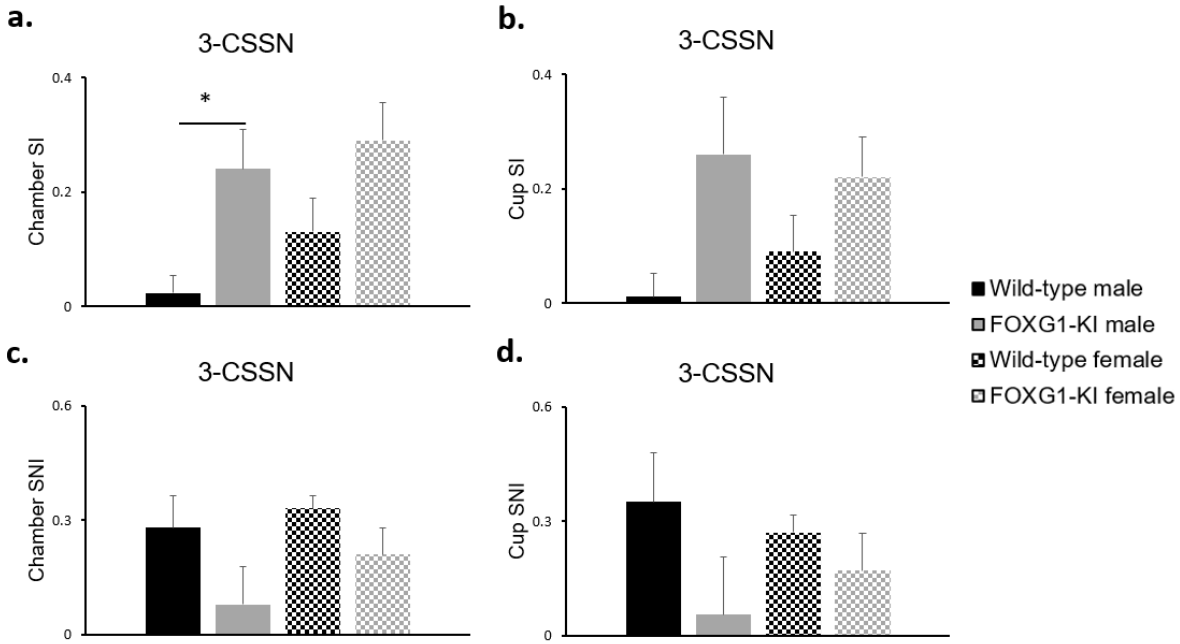

Figure 2.13. Graphs of sociability and social novelty parameters for 3-chamber sociability and social novelty (3-CSSN) test. **a**. Sociability index (SI) based on time in chamber in round 1. SI = [(Time in S1 chamber – time in Emp chamber) / (Time in S1 chamber + time in Emp chamber) **b**. Sociability index (SI) based on time in cup area in round 1. SI = [(Time in S1 cup area – time in Emp cup area) / (Time in S1 cup area + time in Emp cup area)]. **c**. Social novelty index (SNI) based on time in chamber in round 2. SNI = [(Time in S2 chamber – time in S1 chamber) / (Time in S2 chamber – time in S1 chamber)]. **d**. Social novelty index (SNI) based on time in cup area in round 2. SNI = [(Time in S2 cup area – time in S1 cup area) / (Time in S2 cup area – time in S1 cup area)]. (* $p < 0.05$, ** $p < 0.01$, *** $p < 0.001$)

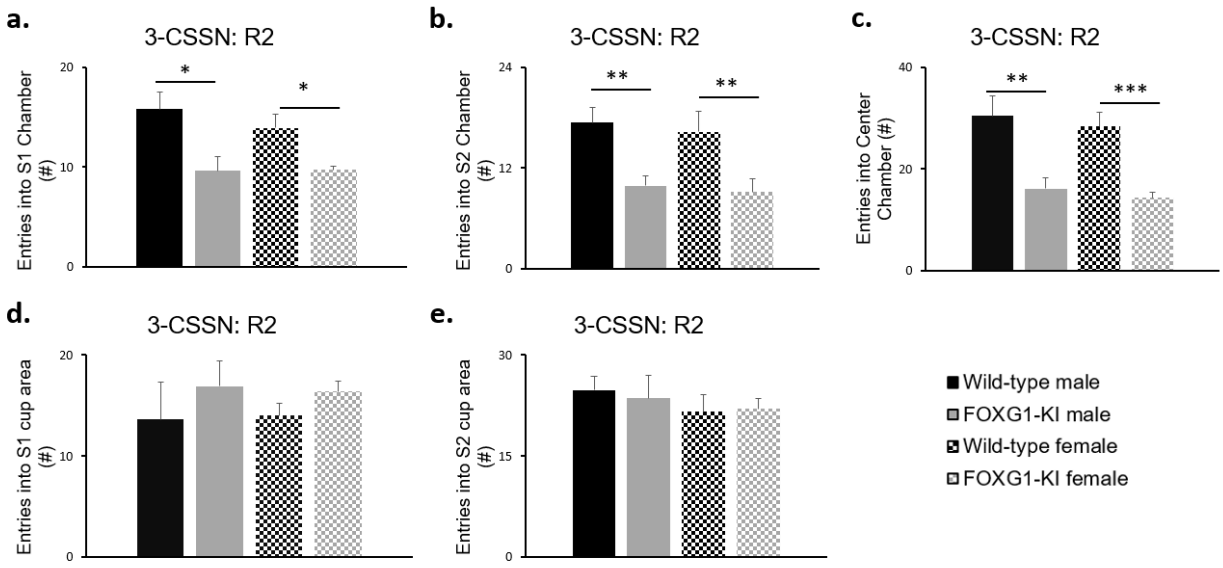

Figure 2.14. Graphs of locomotor activity in 3-chamber sociability and social novelty (3-CSSN) test round 2 (R2). **a**. Entries into S1 Chamber **b**. Entries into S2 Chamber. **c**. Entries into center chamber. d. Entries into S1 cup area. **e**. Entries into S2 cup area. (* $p < 0.05$, ** $p < 0.01$, *** $p < 0.001$)

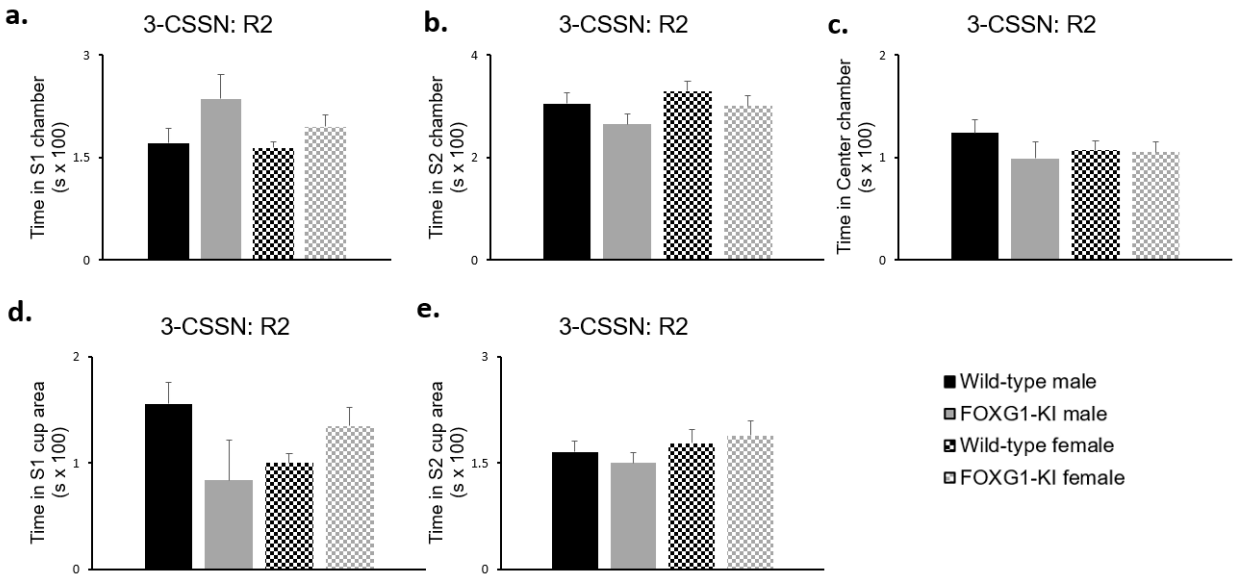

Figure 2.15. Graphs of duration in 3-chamber sociability and social novelty (3-CSSN) test round 2 (R2). **a**. Time in S1 chamber **b**. Time in S2 chamber. **c**. Time in center chamber. d. Time in S1 cup area. **e**. Time in S2 cup area. (* $p < 0.05$, ** $p < 0.01$, *** $p < 0.001$)

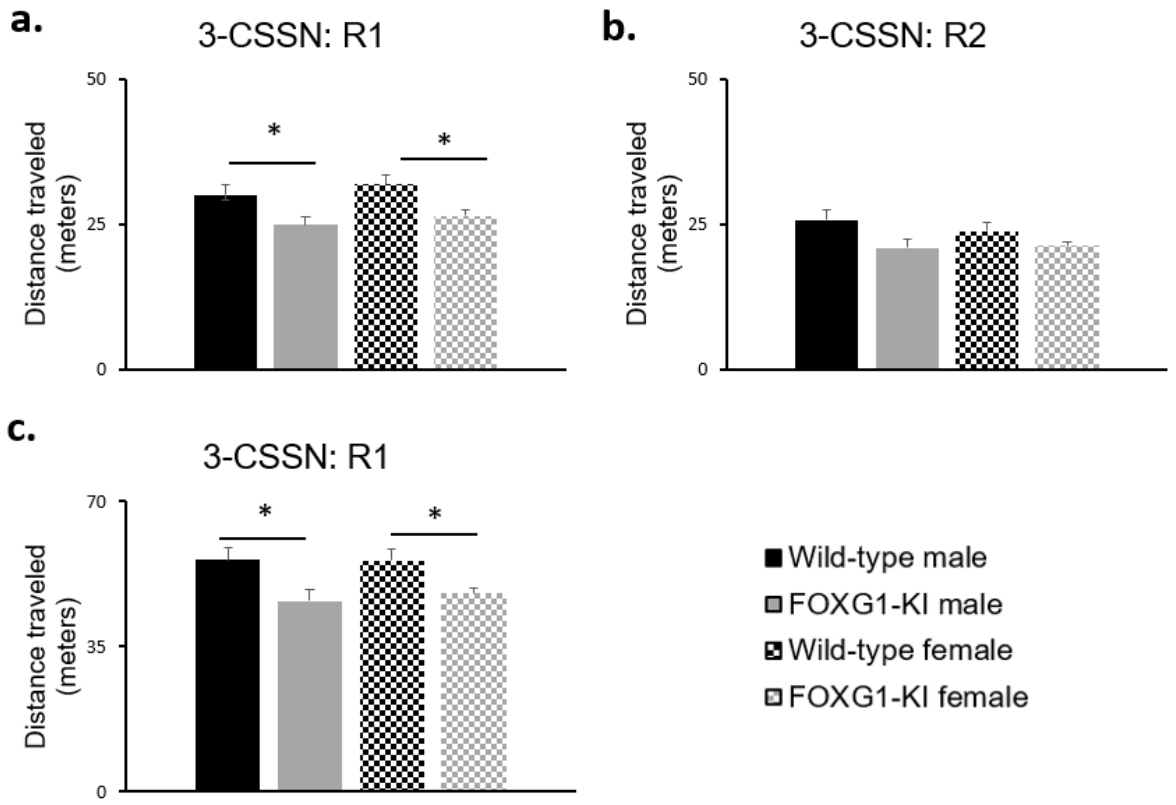

Figure 2.16. Graphs of distance traveled in 3-chamber sociability and social novelty (3-CSSN) test. **a**. Distance traveled in round 1 (R1) **b**. Distance traveled in round 2 (R2). **c**. Total distance traveled. (* $p < 0.05$, ** $p < 0.01$, *** $p < 0.001$)

Behavioral phenotypes: Gait Analysis

To detect the presence of gait dysfunction, I conducted Gait Analysis. I detected significant differences between WT and KI males for forepaw brake time (Figure 2.17.b), forepaw homologous coupling (Figure 2.17.c), hindpaw swing time (Figure 2.18.a), the fraction of hindpaw stride that is stance (Figure 2.18.b), and hindpaw gait angle (Figure 2.18.c). I detected significant differences between WT and KI females for forepaw stance time (Figure 2.17.a), forepaw brake time (Figure 2.17.b), and body rotation (Figure 2.17.d), although the measure for body rotation may be compounded by the WT females being abnormal compared to the other WT animals

The stance time is the amount of time elapsed while the foot is in contact with the runway. The brake time is the time elapsed between the start of a stance and the instance the foot reaches the normal stance position of the front feet, when forced is applied to move the body. The homologous coupling is the fraction of the stride of a reference foot, where the given foot on the same half starts its stride. It is the same as the coordination between left and right foot on the same girdle. The body rotation is the average orientation direction measured in degrees and measures the overall orientation of the animal i.e. the orientation of the body while the animal is walking.

		Male			Female		
Test	Parameter	Wild-type average	FOXG1-KI average	p value	Wild-type average	FOXG1-KI average	p value
GA	Forepaw stance time (ms)	136 ± 3.4	121 ± 6.0	0.088	134 ± 3.5	123 ± 2.5	0.0499
	Forepaw brake time (ms)	65.5 ± 2.1	55.4 ± 3.0	0.031	65.0 ± 1.4	56.3 ± 1.2	0.0015
	Forepaw propel time (ms)	70.3 ± 1.5	65.8 ± 3.6	0.33	68.9 ± 2.4	67.1 ± 1.7	0.58
	Forepaw swing time (ms)	130 ± 4.2	141 ± 5.4	0.19	137 ± 4.4	135 ± 3.6	0.78
	Forepaw stride time (ms)	266 ± 7.0	262 ± 4.7	0.62	271 ± 3.7	259 ± 5.9	0.094
	Forepaw fraction of stride is stance	0.510 ± 0.0056	0.461 ± 0.020	0.071	0.497 ± 0.013	0.478 ± 0.0035	0.26
	Forepaw stride length (mm)	57.4 ± 1.3	30.7 ± 1.2	0.12	56.2 ± 0.80	52.6 ± 1.3	0.13
	Forepaw print area (mm)	127 ± 5.2	114 ± 4.8	0.11	119 ± 4.8	107 ± 1.6	0.066
	Forepaw lateral deviation minimum	5.96 ± 0.10	5.84 ± 0.20	0.66	6.00 ± 0.21	6.01 ± 0.089	0.98
	Forepaw lateral deviation maximum	8.57 ± 0.19	8.57 ± 0.22	0.98	8.51 ± 0.21	8.52 ± 0.055	0.96
	Forepaw longitudinal deviation minimum	5.92 ± 0.21	5.23 ± 0.39	0.20	5.54 ± 0.27	4.91 ± 0.31	0.15
	Forepaw longitudinal deviation maximum	33.5 ± 0.78	31.5 ± 0.86	0.13	32.1 ± 0.36	31.5 ± 0.54	0.36
	Hindpaw stance time (ms)	131 ± 5.0	111 ± 6.9	0.059	122 ± 3.8	113 ± 5.4	0.20
	Hindpaw brake time (ms)	63.3 ± 2.5	57.4 ± 3.1	0.2	57.3 ± 2.5	56.3 ± 4.2	0.82
	Hindpaw propel time (ms)	67.4 ± 3.7	53.7 ± 4.9	0.067	64.8 ± 3.1	57.1 ± 4.2	0.16
	Hindpaw swing time (ms)	139 ± 4.6	161 ± 7.0	0.037	158 ± 13	153 ± 4.8	0.74
	Hindpaw stride time (ms)	269 ± 6.2	272 ± 6.1	0.78	280 ± 11	266 ± 6.7	0.33
	Hindpaw fraction of stride is stance	0.485 ± 0.014	0.412 ± 0.023	0.035	0.449 ± 0.018	0.430 ± 0.014	0.46
	Hindpaw stride length (mm)	57.9 ± 1.4	61.9 ± 1.6	0.11	58.4 ± 2.2	59.9 ± 1.7	0.63
	Hindpaw print area (mm)	199 ± 13	170 ± 7.4	0.067	192 ± 16	194 ± 13	0.94
	Hindpaw lateral deviation minimum	10.2 ± 0.10	9.91 ± 0.17	0.22	9.99 ± 0.13	9.78 ± 0.18	0.35
	Hindpaw lateral deviation maximum	13.0 ± 0.20	12.5 ± 0.32	0.26	12.6 ± 0.19	12.2 ± 0.16	0.14
	Hindpaw longitudinal deviation minimum	8.62 ± 0.34	8.36 ± 0.51	0.71	9.05 ± 0.48	8.05 ± 0.67	0.24
	Hindpaw longitudinal deviation maximum	35.3 ± 0.80	32.9 ± 1.3	0.2	33.6 ± 0.67	33.1 ± 0.84	0.63
	Front track width (mm)	11.4 ± 0.10	11.3 ± 0.36	0.8	11.3 ± 0.39	11.4 ± 0.067	0.86
	Rear track width (mm)	20.5 ± 0.45	19.3 ± 0.45	0.095	19.8 ± 0.30	19.3 ± 0.32	0.26
	Left foot base (mm)	41.3 ± 0.85	39.4 ± 1.6	0.35	38.3 ± 1.2	38.5 ± 1.7	0.93
	Right foot base (mm)	41.1 ± 1.3	38.3 ± 1.2	0.15	41.1 ± 0.74	38.3 ± 1.3	0.067
	Instantaneous running speed (mm/s)	201 ± 1.6	198 ± 4.0	0.61	200 ± 1.2	200 ± 1.1	0.64
	Overall average running speed (mm/s)	202 ± 1.2	199 ± 4.4	0.66	200 ± 1.0	202 ± 1.1	0.17
	Forepaw homolateral coupling	0.517 ± 0.012	0.528 ± 0.010	0.49	0.543 ± 0.0091	0.431 ± 0.012	0.44
	Forepaw homologous coupling	0.498 ± 0.00082	0.491 ± 0.0019	0.021	0.497 ± 0.0025	0.489 ± 0.0047	0.86
	Forepaw diagonal coupling	0.0431 ± 0.010	0.0666 ± 0.011	0.16	0.0682 ± 0.0095	0.0558 ± 0.013	0.45
	Hindpaw homolateral coupling	0.474 ± 0.010	0.444 ± 0.0097	0.066	0.446 ± 0.014	0.462 ± 0.013	0.43
	Hindpaw homologous coupling	0.497 ± 0.0025	0.489 ± 0.0047	0.21	0.491 ± 0.0072	0.492 ± 0.0039	0.91
	Hindpaw diagonal coupling	-0.0156 ± 0.011	-0.0124 ± 0.014	0.87	-0.0299 ± 0.0069	-0.0167 ± 0.013	0.36
	Forepaw gait angle	55.5 ± 0.71	52.5 ± 1.5	0.14	54.2 ± 1.3	53.5 ± 1.5	0.74
	Hindpaw gait angle	68.9 ± 0.75	65.0 ± 1.0	0.018	67.1 ± 0.80	65.6 ± 0.95	0.24
	Body rotation	-0.118 ± 0.57	-1.18 ± 0.77	0.33	0.837 ± 0.46	-1.42 ± 0.75	0.022
	Longitudinal position	75.1 ± 2.6	82.2 ± 2.7	0.096	74.2 ± 2.9	80.8 ± 2.3	0.13
	Lateral position	83.0 ± 0.77	83.3 ± 0.85	0.8	83.5 ± 1.0	83.0 ± 0.73	0.71

Table 2.6. Table containing the averages, SEM, and p values of parameters for the behavioral test gait analysis (GA). p values were calculated using a two-tailed t-test. Significant p values are highlighted in yellow.

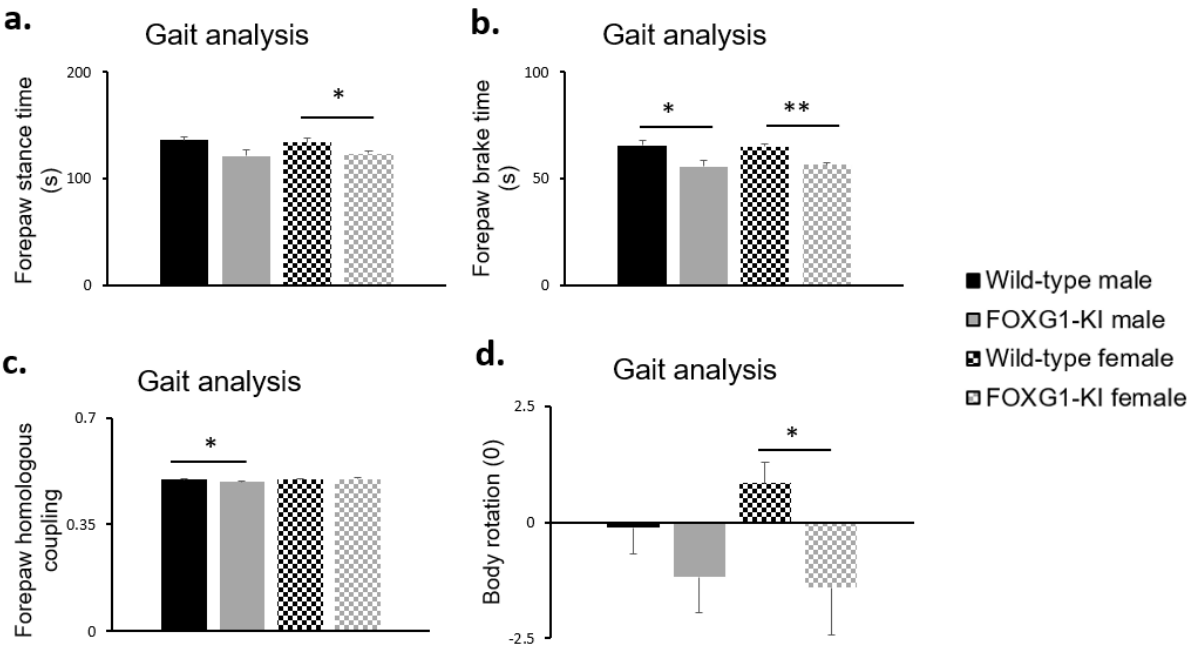

Figure 2.17. Graphs of forepaw and body measures of gait analysis. **a**. Forepaw stance time. **b**. Forepaw brake time. **c**. Forepaw homologous coupling. **d**. Body rotation angle. (* $p < 0.05$, ** $p < 0.01$, *** $p < 0.001$)

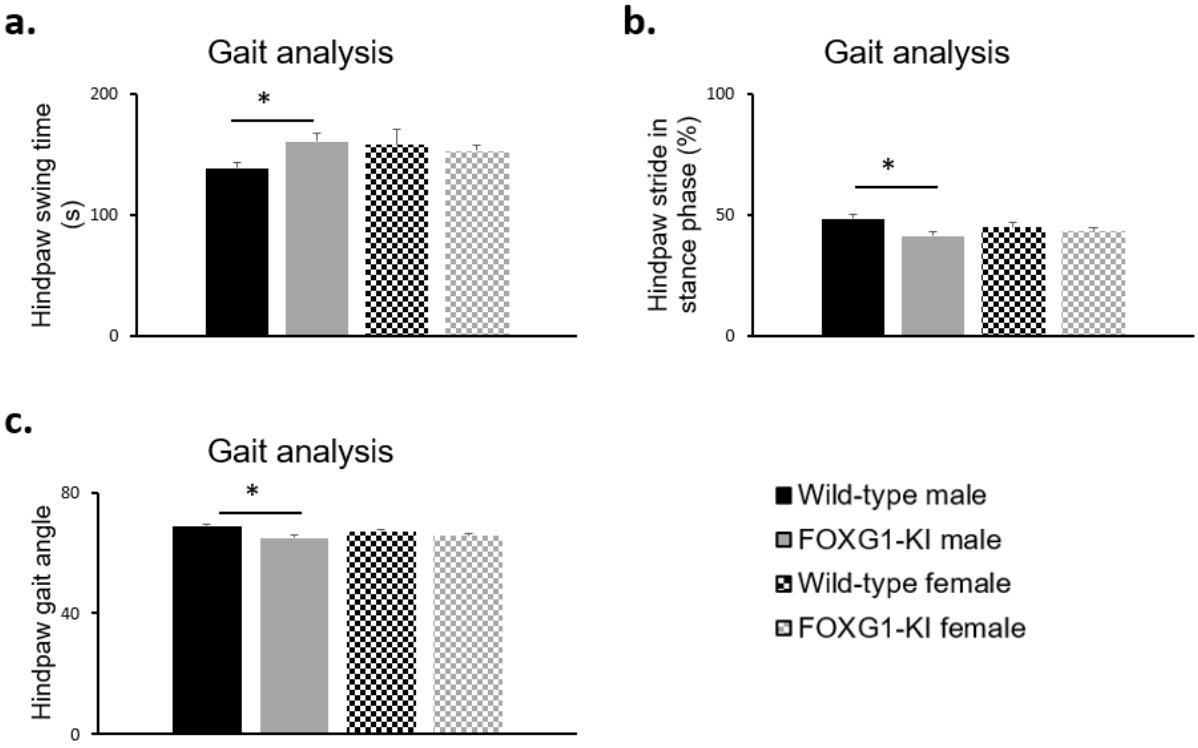

Figure 2.18. Graphs of hindpaw measures of gait analysis. **a**. Hindpaw swing time. **b**. Percent of stride phase in stance. **c**. Hindpaw gait angle. (* $p < 0.05$, ** $p < 0.01$, *** $p < 0.001$)

Behavioral phenotype: resident intruder

To detect changes in aggression, I conducted the resident intruder test. I did this for both male and female mice, introducing them to stranger mice of the same sex. Data is not shown since there was no difference. Of the eight KI male mice, one was attacked and one was an attacker. Of the five WT male mice, one was the attacker. No attacks occurred among the female mice. This leads us to conclude that KI mice have no aggression phenotype.

Discussion and Future Directions

My work provides evidence that our novel FOXG1-KI mouse model is applicable to recapitulate in part the phenotypes associated with FOXG1 Disorder. Our mouse model has decreased FOXG1 protein levels in the whole brain and structural abnormalities of the corpus callosum and hippocampus. These mice also significantly exhibit hypoactivity in both males and females, increased anxiety, in males and females, decreased motor learning in females, increased memory in females, and some gait abnormalities for both males and females. What was unexpected was the presence of an increase in object memory in the female KI animals. However, this may be accounted for by the overall increase in time spent investing objects in the NOR task. In the 3-CSSN task the males exhibit increased sociality in one parameter (Chamber) but not another (Cup). The Cup measurement is a more stringent parameter and that should be trusted more.

Overall, I suggest that a repeat of some behavioral parameters with different tests is necessary to thoroughly demonstrate the relevance of this mouse model for studying FOXG1 Disorder. For example, the differences in memory could be tested again using the object location memory test and anxiety could be tested again using the elevated zero maze. Repeating my IHC with a larger group and capturing images with a confocal microscope is also suggested, performing more detailed quantification of hippocampal abnormalities, looking at neuronal markers, as well as examining other brain regions.

CHAPTER 3

VALIDATION OF THE SUCCESS OF RECOMBINATION OF FOXG1-HA GENE

Introduction

FOXG1 Disorder, with only 100 currently known cases, is rare enough that the mutations are not on a panel for genetic testing *in utero*. In a study conducted by Vegas et al. 2018, five out of forty-five subjects exhibited prenatal brain anomalies. The average age the individual with FOXG1 Disorder is diagnosed with any neurodevelopmental impairments is three months of age due to marked developmental delays. Because there is no current treatment there is no particular reason to identify cases pre-symptomatically. However, recent work in other related neurodevelopmental disorders such as Rett syndrome has demonstrated that restoration, even post-symptom onset, can reverse symptoms (Guy et al. 2007). This has led to the development of gene therapy in Rett syndrome, and the question remains whether similar re-expression of *FOXG1* postnatally could partially ameliorate or completely resolve clinical features of the Disorder.

One of the aims with this project was to investigate the possibility of remediation of some of the phenotypes associated with the Disorder by restoration of wild-type levels of *FOXG1* using a genetically engineered mouse model, FOXG1-KI (presented in detail in chapter 2). A significant question is when during development re-expression of *FOXG1* would be sufficient to improve phenotypes, and the work proposed here was meant to determine whether effective phenotypic rescue can be achieved via embryonic, early post-natal, or juvenile re-expression. This will help determine the optimal timing of potential therapeutics.

To explore the ability of this new FOXG1-KI line to re-express wild type levels of *FOXG1* and to rescue phenotypes, I generated two lines by mating KI to transgenic Cre lines that

express Cre at different time points in different tissues, which should cause recombination of FOXG1-KI to express FOXG1 protein tagged with an epitope (HA).

In order to generate animals that have permanently recombined the *FOXG1-KI* allele to express *FOXG1-HA*, I have crossed FOXG1-KI with a HoxB1-Cre animal, where Cre recombinase expression is driven by the promoter to the HoxB1 gene. Some animals that possess both the *FOXG1-KI* and the *HoxB1-Cre* genes develop germline mutations, so the permanently recombined allele can be passed to offspring. This creates a new line that is called FOXG1-HA, where the FOXG1-HA protein should be expressed whenever endogenous FOXG1 is expressed. The mice in this line carrying one *FOXG1-HA* gene are said to have the genotype of HA. An HA tag is a portion of the protein Human influenza hemagglutinin. It is a commonly-used epitope tag that should be recognized by commercially available antibodies against HA, providing a read-out of successful re-expression of FOXG1 protein. We have engineered the reinstated FOXG1 protein to be tagged with HA as a positive control, as proof that the protein is being expressed correctly, and that after recombination the mice are phenotypically normal

The second line was generated to determine if early embryonic recombination could successfully express *FOXG1-HA* and rescue phenotypes found in KI animals. To this end, I was to cross our FOXG1-KI line with lines where Cre recombinase is driven by the timely expression of specific developmental genes. I already possessed one of those lines and had established the FOXG1-KI/Cre line FIN. FIN is a FOXG1-KI animal crossed with a Nestin-Cre animal, where Cre expression is driven by the promoter to the *Nestin* gene. Animals in this line carrying both *FOXG1-KI* gene and the *Nestin-Cre* gene are called to have the genotype “KI; Nestin-Cre.” The expression of *Nestin* commences around E7.5, before *FOXG1* expression is supposed to begin. Through the use of this line, we will be able to determine what phenotypes are rescued following Cre excision of the stop cassette prior to the expression of *FOXG1*.

Western blotting

For an effort towards proof-of-principle, I ran many western blots (WB) to probe for the HA tag. See Table 3.1 for a summary of the conditions by which I performed WB for this purpose. For the majority of the WB, 10 ug of protein isolated from mouse hemibrain was loaded into each well. The usual dilution factor for chicken anti-HA (Abcam, cat no ab134028), mouse anti-HA (Cell Signaling, cat #2367), and mouse anti-HA.11 (Biolegend, cat no 901513) was 1:1000. The dilution factor for rabbit anti-FOXG1 (Abcam, cat no ab18259) was 1:500. The HA antibodies were verified as functional using a Sox2-HA plasmid from Addgene (cat no 13459, pCAG-HA-Sox2-IP), the protein of which is expressed in and isolated from HEK293 cells to produce a positive control HA tag epitope (Figure 3.1.a, Lane 13, Band 1) which is fused to Sox2 protein (Figure 3.1.b, Lane 13, Band 1). I isolated the protein using RIPA buffer and used protein isolated from non-transfected HEK293 cells as a negative control (Figure 3.1, Lane 14).

		Iteration	1	2	3	4	5	6	7	8	9	10	11	12	13	14	15	16	17	18
Sample	KI; Nestin/Cre	Male	x	x	x	x	x		x	x	x	x	x	x	x					
		Female																		
	KI; Hoxb1/Cre	Male																	x	
		Female						x	x	x	x	x	x	x	x				x	
	WT; WT	Male			x	x				x	x	x	x	x	x	x	x	x	x	x
		Female														x	x	x	x	x
	KI; WT	Male	x	x	x	x	x		x	x	x	x	x	x	x				x	
		Female																	x	
	FOXG1-HA	Male														x	x	x		x
		Female														x	x	x		x
	HEK293	Sox2-HA (+ control)											x	x	x				x	x
	Age	Fetus														x	x	x		x
		Young (< 4 mos)						x	x	x	x	x	x	x	x				x	
	Tissue	Old (> 4 mos)	x	x	x	x	x		x	x	x	x	x	x	x		x	x		
		Hippocampus						x	x	x	x									
		Hemibrain	x	x	x	x	x	x	x	x	x	x	x	x	x		x	x	x	x
	Method of extraction	RIPA						x	x	x	x		x						x	
		Nuclear fractionation	x	x	x	x	x	x	x	x	x	x	x	x	x	x	x	x		x
Gel composition	Pre-made	Bio-Rad 4-20% 15 well P10019359					x	x		x	x		x	x	x	x	x		x	x
		Bio-Rad 4-20% 10 well, P4561094							x											
	Hand-poured	10% acrylamide running gel	x	x	x	x						x						x		
Gel run	95 V	~ 2.5 hours	x	x	x							x						x		
	200 V	45 minutes					x	x	x	x	x		x	x	x	x	x		x	x
Transfer	200 mA	1 hour				x	x	x	x	x	x	x	x	x	x	x	x		x	x
		2 hour	x	x	x													x		
Probing	HA antibody	Chicken anti HA			x	x	x	x	x	x		x	x	x	x	x	x	x	x	
		Mouse anti HA	x	x	x			x			x									
		Mouse anti HA.11																	x	x
	Foxg1 antibody	Rabbit anti Foxg1	x	x	x	x	x	x	x	x	x	x		x	x	x	x	x	x	x
	Buffer	Blocking buffer	x	x	x	x	x	x	x	x	x	x	x	x	x	x	x	x	x	x
	Secondary	Gt anti Rb 800	x	x	x	x	x	x	x	x	x			x	x	x	x	x	x	x
		Goat anti Mouse 680	x	x	x			x			x								x	x
		Donkey anti chicken 680			x	x	x	x	x	x			x	x	x	x	x	x	x	

Table 3.1. Details of iterations of western blots that have been run.

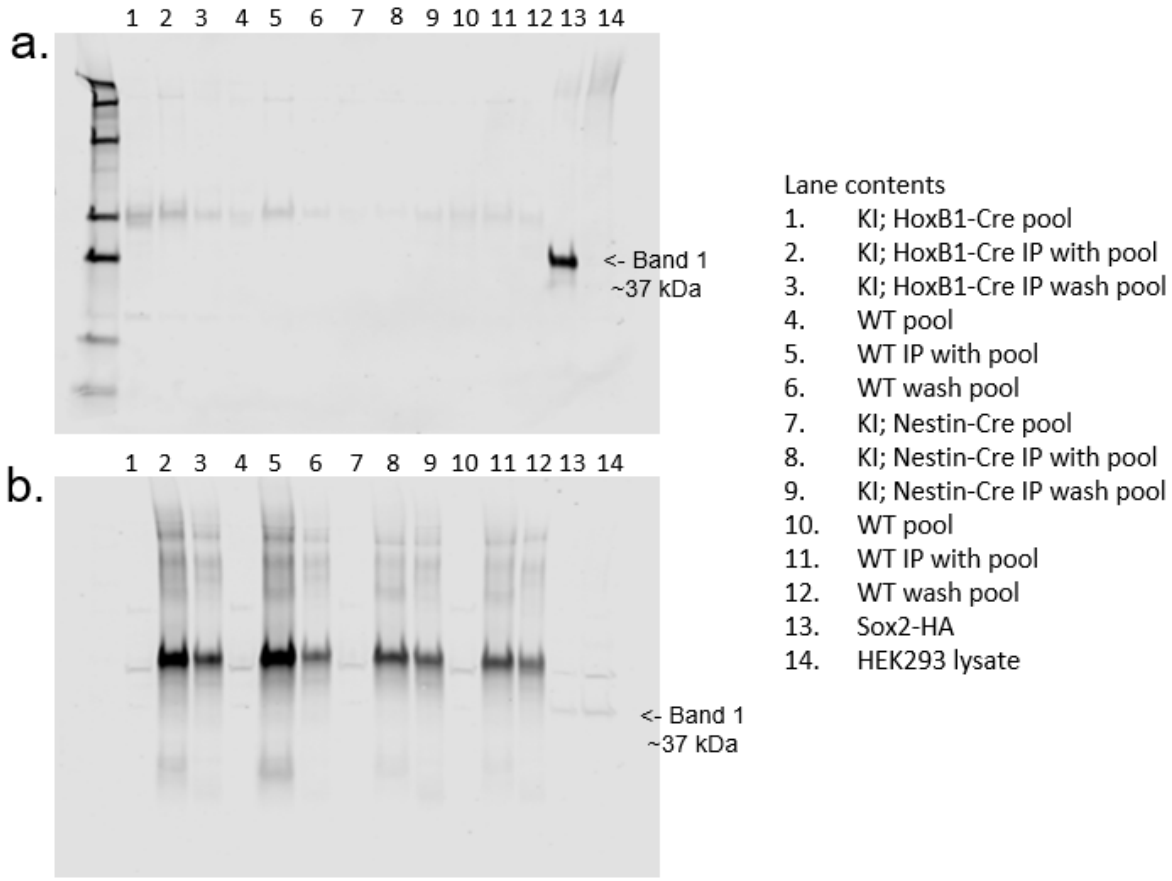

Figure 3.1. Western blot with HA epitope antibody positive control. **a**. Immunostaining with anti-HA. Band 1 is the HA tag fused to the positive control protein samples Sox2-HA. **b**. Immunostaining with anti-Sox2. Band 1 is the protein Sox2. Pool = pool of equal amounts of nuclear and cytoplasmic fractions of protein lysates.

In summary, a band that was the correct molecular weight for the HA tag was present in some samples isolated from mouse brains. However, this band also was present in WT samples (Figure 3.2.a, all lanes, Band 1). In the iterations with FOXG1-HA embryos, a separate band around 70 kilodaltons (kDa) was present for anti-FOXG1 (Figure 3.3.b, Band 1, lanes 1, 3, 5, 7, 9, 11). It is possible that this is a phosphorylated version of FOXG1 (pFOXG1). When probing for HA, a faint band around 47 kDa was present for all samples, including WT (Figure 3.3.a, Band 2, all lanes). However, where pFOXG1 may be there is a doublet band in the HA animals (Figure 3.3.a, Band 1, lanes 1 and 3). In all WB, there is more FOXG1 protein present in cytoplasmic fractions than nuclear fractions (Figure 3.2).

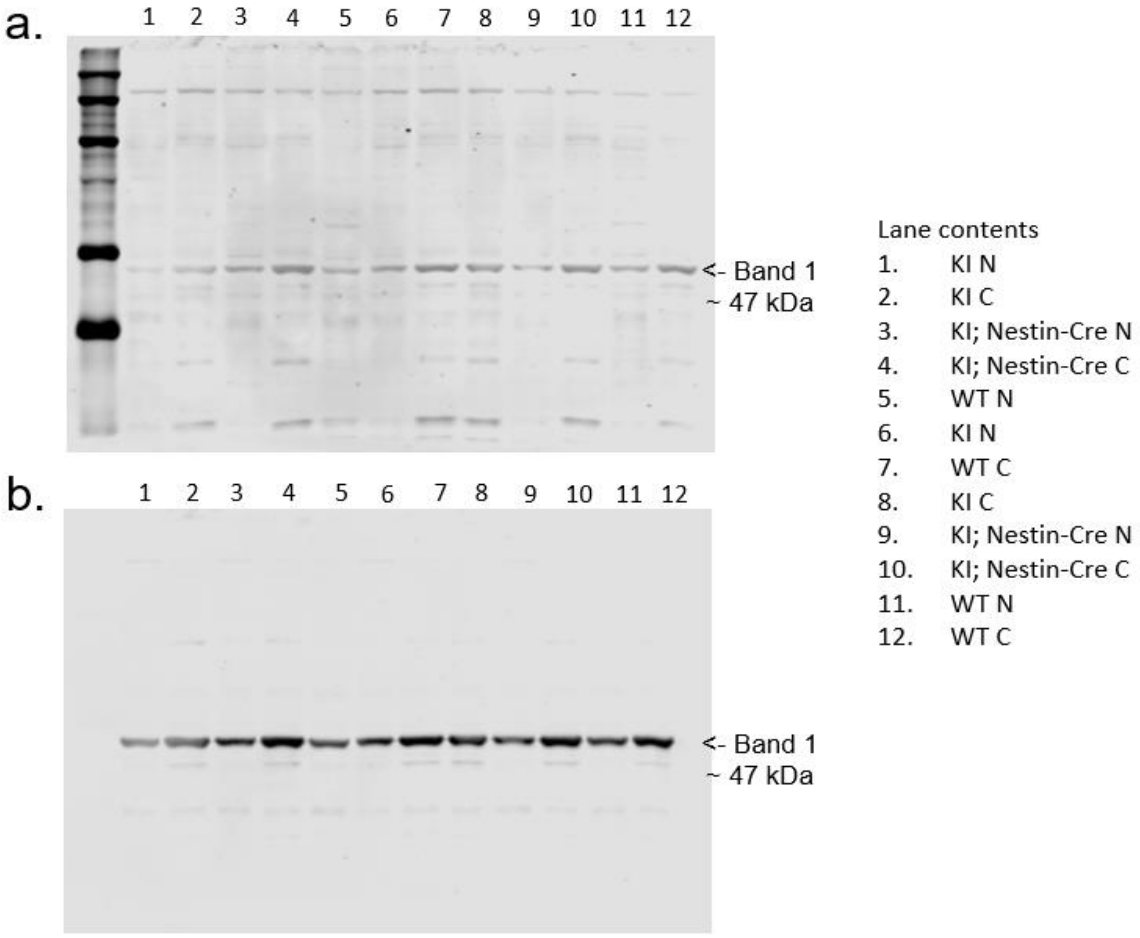

Figure 3.2. Western blot highlighting presence of HA band in wild type as well as KI; Nestin-Cre lysates. **a**. Immunostaining with anti-HA antibody. Band 1 is the expected MW of the HA tag. **b**. Immunostaining with anti-FOXG1 antibody. Band 1 is the protein FOXG1. N = nuclear fraction, C = cytoplasmic fraction

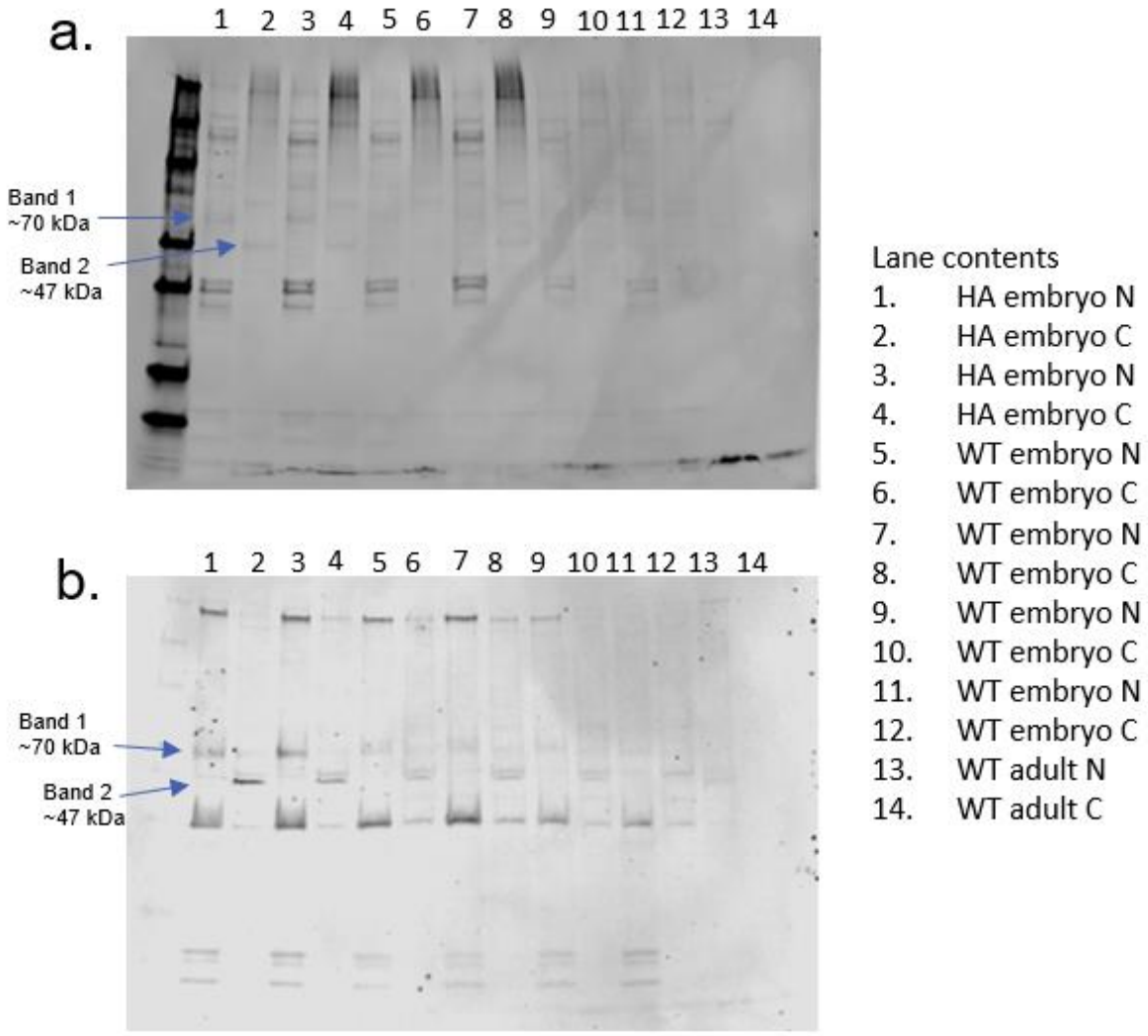

Figure 3.3. Western blot of FOXG1-HA and WT embryos highlighting the potential presence of phosphorylated FOXG1 protein. **a**. Immunostaining with anti-HA antibody. Band 1 is potentially phosphorylated FOXG1 protein. Band 2 is potentially FOXG1-HA. **b**. Immunostaining with anti-FOXG1 antibody. Band 1 is the protein is potentially phosphorylated FOXG1. Band 2 is FOXG1. N = nuclear fraction, C = cytoplasmic fraction

Immunoprecipitation

Since I did not see the presence of FOXG1-HA on a WB, I assumed that the levels of FOXG1-HA may be too low. Thus, I conducted immunoprecipitation reactions (IP). I used beads, both agarose and magnetic, that had been incubated with rabbit anti-FOXG1 or chicken anti-HA, or rabbit anti-MeCP2 (Cell Signaling, cat #3456) as a negative control. See Table 3.2 for the different iterations. This was in an effort to concentrate the FOXG1 protein since only so much protein could be loaded onto a WB depending on the concentration of the original lysate sample. I conducted the IP procedure followed by elution in 2x sample buffer. I loaded the samples into a protein gel, along with original sample, post-antibody pre-wash sample, and a wash sample as controls.

			1	2	3	4
Sample	KI; Nestin/Cre	Male	x	x	x	
	KI; WT	Male	x	x	x	
	KI; Hoxb1/Cre	Female			x	x
	WT; WT	Male			x	x
	HEK293	Sox2-HA				x
	Lysate	Nuclear	x	x		
		Pool of nuclear and cytoplasmic			x	x
Procedure	Buffer	B	x	x	x	x
	Beads	Agarose	x			
		Magnetic			x	x
	Antibody dilution	1:100	x		x	x
		1:50		x		
	Antibody	Rabbit anti foxg1	x	x	x	x
		Rabbit anti D4F3		x		
		Mouse anti HA				x
	Wash	Buffer B	x		x	x
		TBST		x		
	Input volume	100 ul	x			x
		250 ug		x	x	
	Elution volume	30 ul	x		x	x
		100 ul		x		
	Treatment	Elution heated	x			

Table 3.2. Details of iterations of immunoprecipitations that have been run.

FOXG1 did not appear definitively in any of these iterations. I believe that the concentrated presence of IgG, with a heavy chain of 50 kDa, is obscuring the presence of FOXG1 (Figure 3.4.b, Band 1). Lanes 2 and 3 of Figure 3.4.b, for example, have rabbit anti-FOXG1 antibody already in the samples. This IgG theory is supported by the presence of smears around 25 kDa, which is the molecular weight (MW) of the light chain of IgG (Figure 3.4.b, Band 2). The IgG interfering with FOXG1 protein staining is further evidenced with an IP using the MECP2 antibody that did not result in such a large smear around this MW (Figure 3.4.b, Band 1, lane 7). In addition, an IP performed with an HA antibody did have a band around 50 kDa, suggesting the presence of IgG, but did not have the longer smear that is seen in the IPs completed with the FOXG1 antibody (Figure 3.5.b, Band 1). Regardless of if that band does contain FOXG1, it is not quantifiable.

When I used the HA antibody for the IP as well as the positive control sample Sox2-HA, I found that a faint band around 37 kDa was present in the channel I used to probe for mouse anti-HA (Figure 3.5.a, Band 1), making the use of the IP procedure inconclusive on if it worked. For all iterations of the IP procedure there was no definitive HA signal, as the signal that may be taken for HA has the correct MW and appears in the correct channel, was present in the WT samples as well (Figure 3.4.a, Band 1).

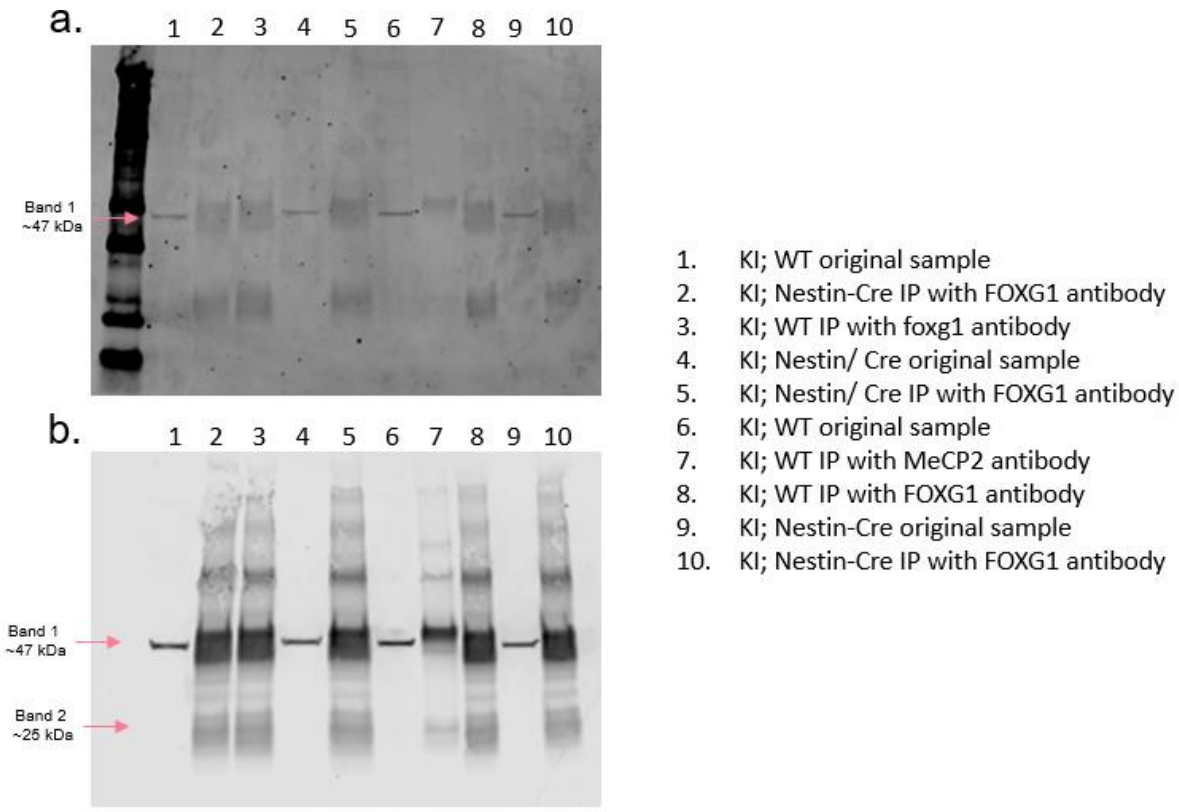

Figure 3.4. Western blot of immunoprecipitation procedure completed with FOXG1 and MECP2 antibodies highlighting the potential of rabbit IgG signal interfering with FOXG1 signal. **a**. Immunostaining with anti-HA antibody. Band 1 was initially believed to be FOXG1-HA. **b**. Immunostaining with anti-FOXG1 antibody. Band 1 and Band 2 are potentially heavy and light chains of rabbit IgG, respectively

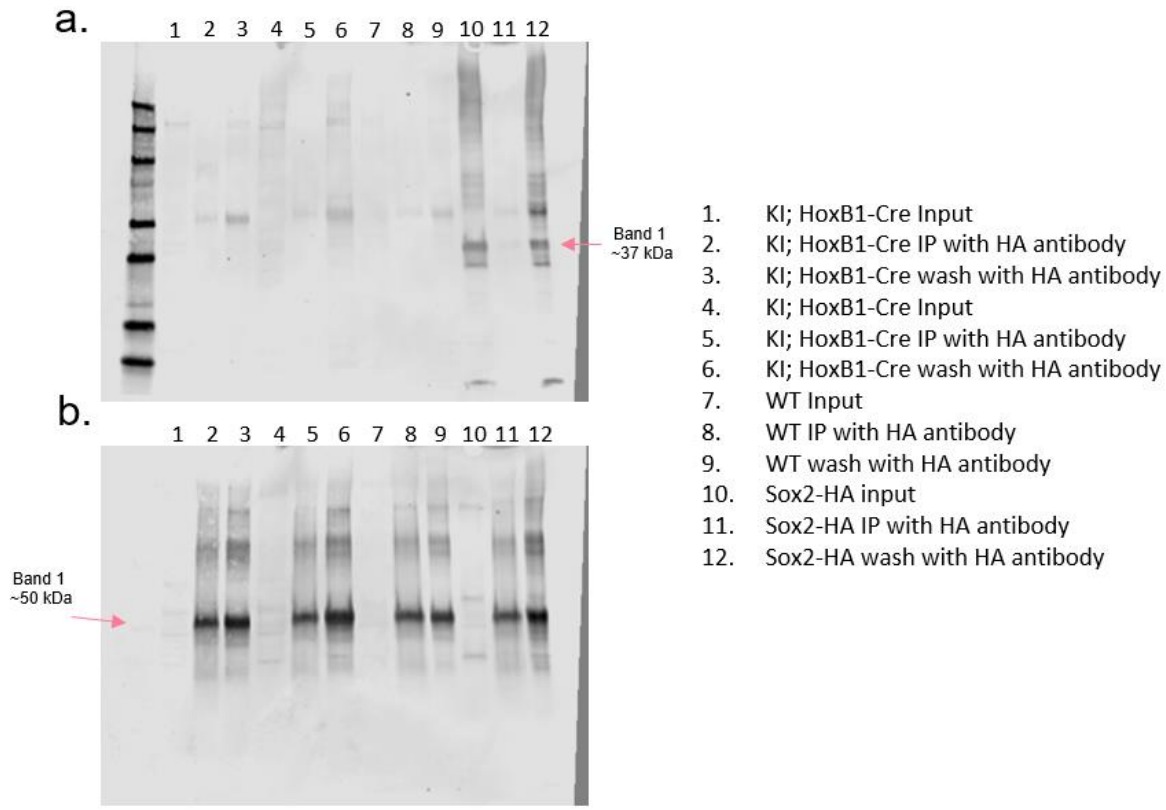

Figure 3.5. Western blot of immunoprecipitation procedure completed with mouse anti-HA antibody, highlighting the potential presence of rabbit IgG interfering with FOXG1 signal. **a**. Immunostaining with anti-HA antibody. Band 1 is Sox2-HA. **b**. Immunostaining with anti-FOXG1 antibody. Band 1 is potentially rabbit IgG.

In summary, it is inconclusive if the IP reactions worked. It is difficult to determine when running the IP reaction with anti-FOXG1 antibody due to only possessing one anti-FOXG1 antibody, since no other antibody has been found to be as consistently effective. Precipitating with one antibody (such as rabbit anti-FOXG1) and using an antibody in that same species leads to the secondary antibody significantly highlighting the whole sample due to the secondary associating with the IgG of that species in the sample. The IP reaction using anti-HA antibody was not definitive either.

Sequencing

The next step was to sequence the gene. There was a possibility that the stop cassette (SC) or splice acceptor (SA) had been placed in the wrong sequence, or that what was fused to the FOXG1 protein was a tag different from HA. To verify that the SC and SA were present I designed primers overlapping an area of the 5'UTR of the FOXG1 gene (Figure 3.6, primers Foxg1_5utr_f1 and Foxg1_5utr_r1). To verify the presence of the HA tag I designed primers to overlap the C-terminus (c-term) region of FOXG1 where the HA tag was supposed to be present (Figure 3.6, Foxg1_cterm_f1 and Foxg1_cterm_r1).

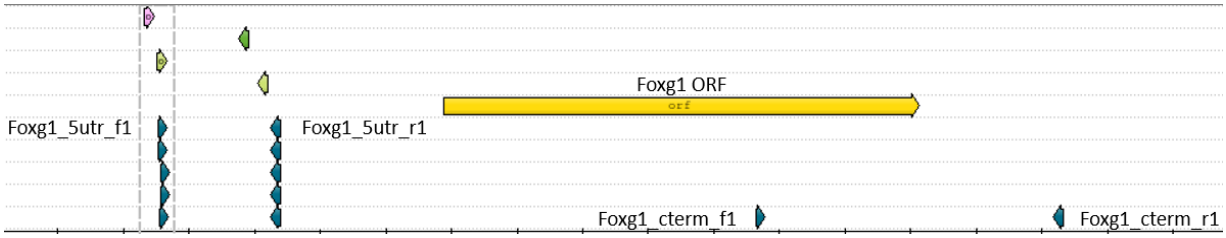

Figure 3.6. Sequencing primers in relation to *FOXG1* open reading frame (ORF)

I isolated DNA from a KI; HoxB1-Cre animal with the DNeasy blood and tissue kit (Qiagen cat. no 69504) followed by amplifying the specific sequences using the Phusion U Hotstart PCR master mix kit (Thermofisher, cat no F553L). I ran the product of this reaction on a gel to verify the reaction worked. I expected one band for the 5'UTR primers around 300 base pairs (bp), and two bands for the cterm primers, one at 800 bp and the second at 1000 bp. There were multiple bands for the c-term primers between 600 and 1200 bp but no band for the 5'UTR primers (Figure 3.7). I followed this with troubleshooting the amplification step using a gradient for the annealing temperature, differing extension times, increasing the template, and more. I ran the product of this protocol out on a gel and cut out bands at pre-determined lengths listed above using a UV light box. I did not excise the band for the 5'UTR due to there not being a band prominent enough to visualize on the light box. I isolated the cterm bands using a Wizard SV gel and PCR-clean up system (Promega, cat. no A9281). I concentrated the cterm product using the Purelink Quick PCR purification kit (Invitrogen, cat no K310002) and ligated it onto a U6 backbone using a T4 DNA ligase enzyme (New England BioLabs, cat no M0202S). I sent this for sequencing at GenHunter with the Foxg1_cterm_f1 primer. This sequence is slightly different than the conventional HA tag sequence. I found an antibody (mouse anti HA.11 epitope tag) that is specific to that sequence, which I listed as using in Table 1.

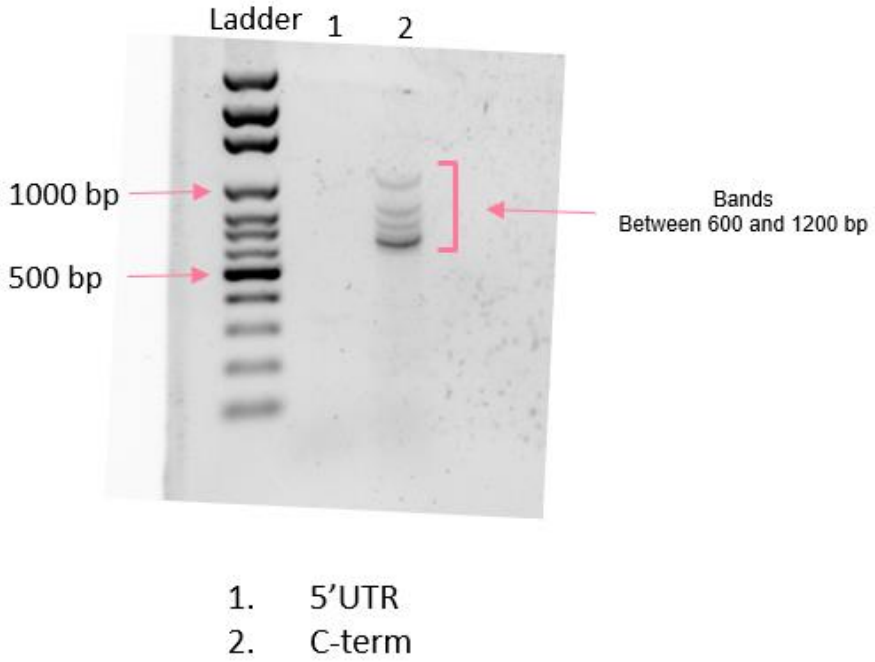

Figure 3.7. Image of agarose gel that has contains PCR product made using sequencing primers Foxg1_5utr and Foxg1_cterm

Immunohistochemistry

To search for the HA tag through a different method, I attempted to visualize FOXG1 in an anatomical context. There is a possibility that the HA tag could be cleaved by caspases while being isolated through the method of protein extraction (insert citation). See Table 3.3 for the iterations of IHC I performed, including adults and embryos, differing section thickness, forgoing fixative, the different HA tag antibodies I possess, and more. I used the HA tag antibodies at a range of dilution factor from 1:250 to 1:1000 for all antibodies. FOXG1 protein signal was visible under all conditions but is visualized best under the sodium-citrate antigen retrieval method. I initially believed I had visualized the HA tag on the first iteration. However, the signal did not co-localize with the FOXG1 signal. Other iterations did not have this signal. There are many more ways to perform this method, but as of now the HA tag has not been successfully visualized.

			1	2	3	4	5	6
Sample	KI; Nestin/Cre	Male	x	x				
	KI; Hoxb1/Cre	Female					x	
	FOXG1-HA	Embryo			x	x		x
	WT	Embryo			x	x		x
	Cut	Section thickness	35 um	35 um	30 um	30 um	10 um	40 um
		Sagittal	x	x			x	x
		Coronal			x	x		
Method	Condition	Antigen retrieval						x
		No fixative					x	
		Wash with Triton-X					x	x
	Antibodies	Rabbit anti FOXG1	x	x	x	x	x	x
		Chicken anti HA		x	x	x	x	
		Mouse anti HA.11						x
		Mouse anti HA	x	x		x	x	x

Table 3.3. Details of iterations of immunohistochemistry that has been performed.

Vector cloning

Some of the big questions with this FOXG1-HA protein is if it can be expressed, if it is stable after being expressed, if it folds correctly, and more. To address some of these potential issues I started working on a vector cloning project. The theory behind this is to ligate a gene into a mammalian expression vector that will be transfected into mammalian cells. The protein can then be overexpressed and isolated for further testing. The plan was to start by isolating RNA from two animals: a KI; HoxB1-Cre animal and a WT animal. I would make a cDNA library from the RNA with oligo(dT)s and use primers to amplify the desired sequence. The forward primer is sense to the mRNA and starts at the start codon of the *FOXG1* mRNA (cloning_primer_F1) and the reverse primer is antisense to the mRNA and ends after the HA tag but is still in the predicted 5'UTR of the *FOXG1* mRNA (cloning_primer_R1) (Figure 3.8). The reverse primer is the same one we use for genotyping for the presence of the HA tag. The product should be around 1,500 bp. Following this, I would use two sets of nested primers to add the attB sequences (attB1 followed by attB2). I would then to ligate this PCR product into a pDONR plasmid that contained attP sites using BP Clonase II. I would grow up the plasmid and transfect it into HEK293 cells and isolate protein to verify the FOXG1-HA protein was expressed.

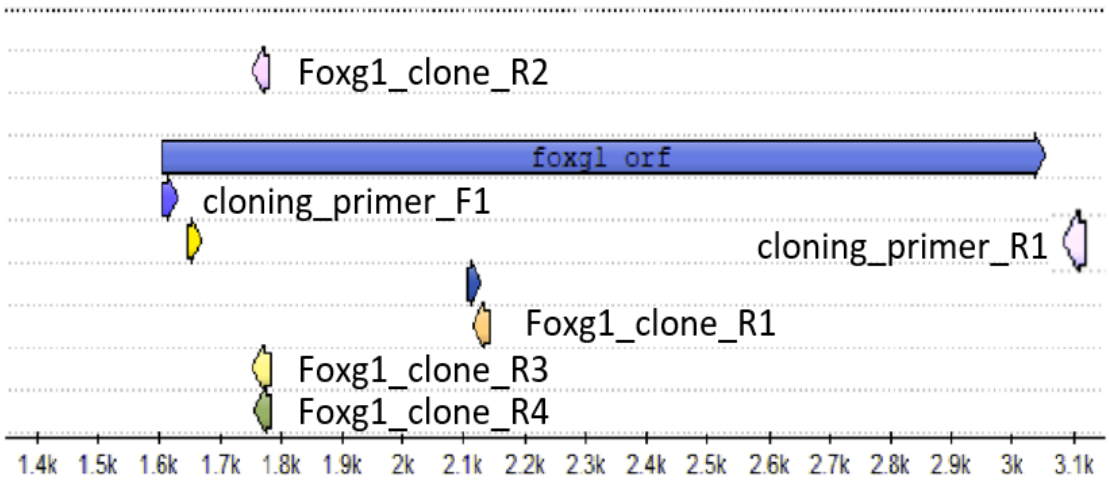

Figure 3.8. Image of cloning primers in relation to ORF of *FOXG1* gene.

Towards this plan, I successfully isolated RNA from the two animals using the Direct-zol RNA miniprep kit (Invitrogen, cat no R2050). RNA was taken from the hippocampus and cortex for both animals. I used to Superscript IV first-strand synthesis kit (Invitrogen, cat no 18091) to make a cDNA library using dNTPs. I followed this by using the Kapa Hifi PCR kit (Kapa Biosystems, cat no KR0368) to amplify the sequence using the primers cloning_primer_f1 and cloning_primer_r1. Following rounds of troubleshooting using the PCR kit with different cycle numbers, annealing temperature, extension times, etc., I ran each PCR product on a gel and visualized either no product or product of the incorrect size (Figure 3.9). I tried the procedure with DNA isolated from a KI; Nestin-Cre animal and had the same result (Figure 3.10). I validated the functionality of the cloning_primer_f1 by purchasing a reverse primer 200 bp downstream of the primer (Figure 3.8) and ran an Econotaq genotyping reaction, which resulted in a product of the correct size (Figure 3.11).

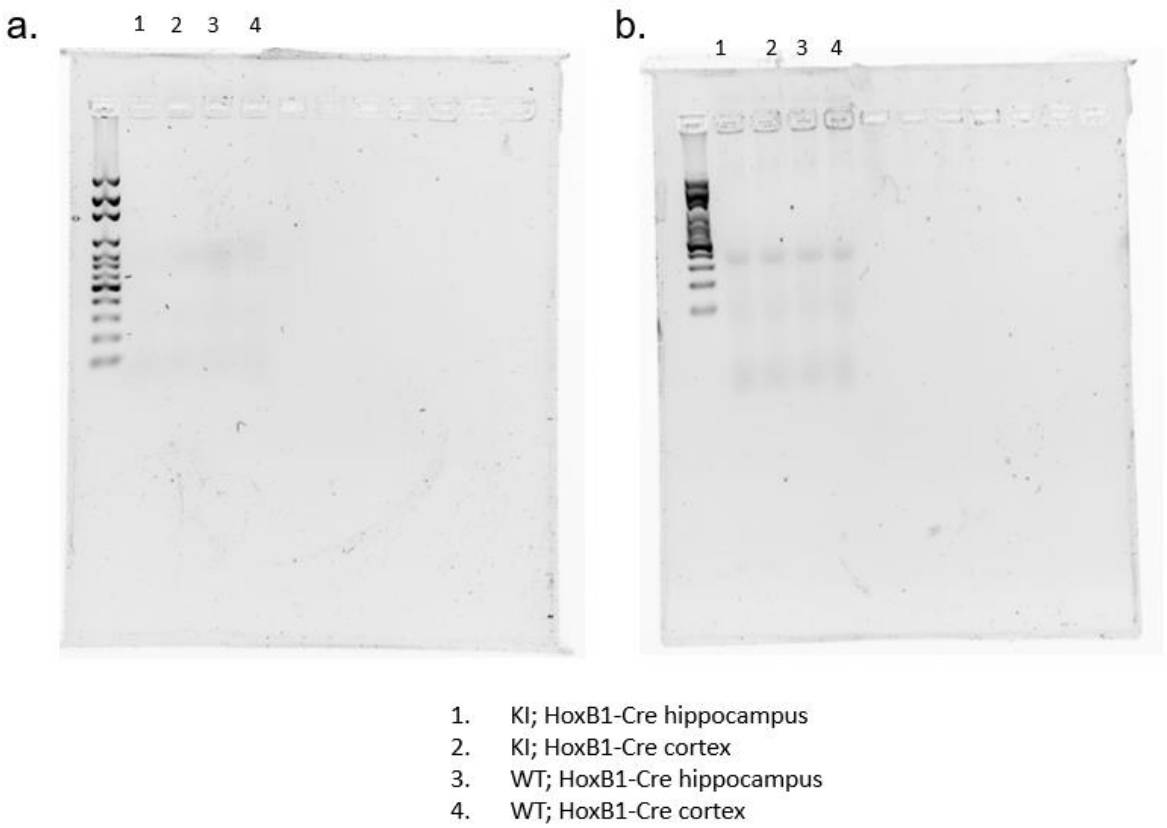

Figure 3.9. Image of agarose gel that has PCR product from reactions using cloning_primer_F1 and cloning_primer_R1 and cDNA generated from mRNA. **a**. PCR run containing no product. **b**. PCR run containing product of incorrect molecular weight.

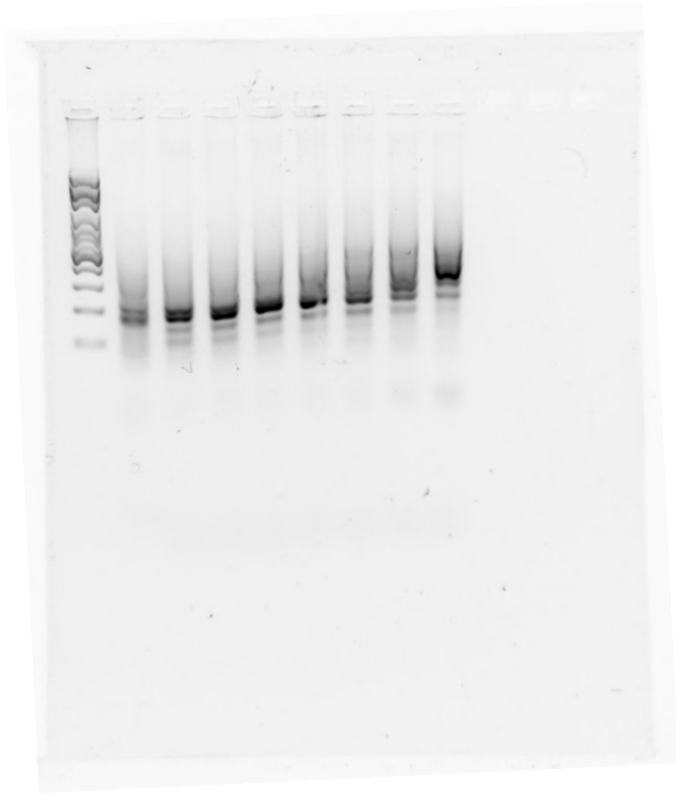

Figure 3.10. Image of agarose gel that has PCR product from reactions using cloning_primer_F1, cloning_primer_R1, and tail lysate from a KI; Nestin-Cre animal.

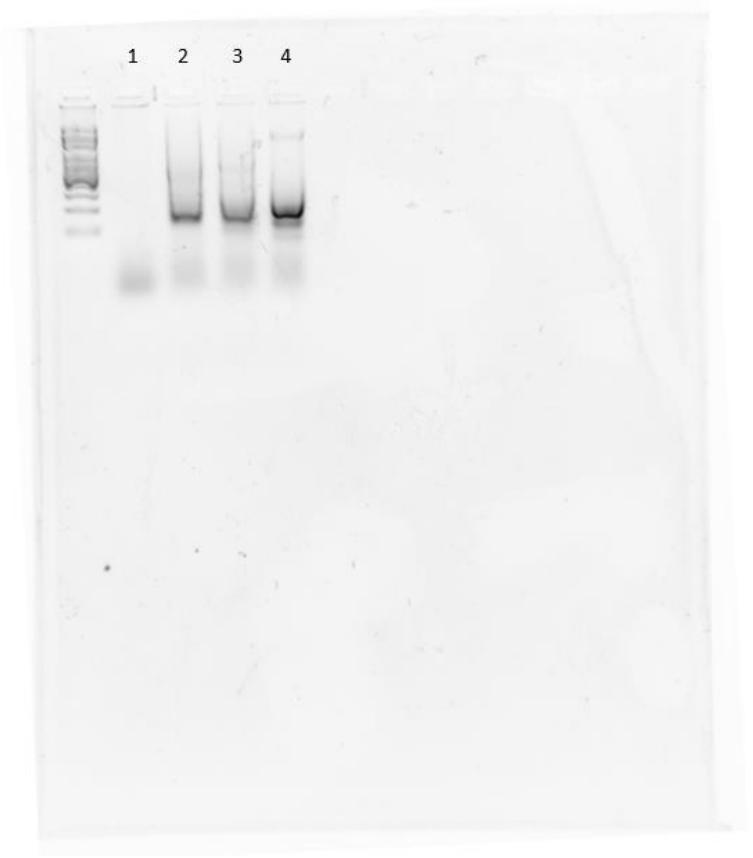

Figure 3.11. Image of agarose gel that has PCR product from reactions using cloning_primer_F1 and Foxg1_clone_R1 (lane 1), Foxg1_clone_R2 (lane 2), Foxg1_clone_R3 (lane 3), and Foxg1_clone_R4 (lane 4).

At this point, Dr. Neul suggested a new way I could complete the task of having the HA tag expressed on the FOXG1 protein. The new plan was to purchase a plasmid already containing the *FOXG1* gene. I would use restriction digests to excise the C-term region of *FOXG1* and ligate in PCR product containing the HA tag and transfect that product into HEK293 cells for expression. I purchased a Myc-DDK tagged *FOXG1* (Origene, cat no MR207714, Figure 3.12.a) for this purpose. For the HA tag sequence, I already had the sequence inserted into a U6 plasmid that I had made for the purpose of sequencing. I found two restriction digest sequences bracketing the c-term sequence of the *FOXG1* I wanted to excise, as well as the sequence of placement of these restriction digest sequences in comparison to the *FOXG1* gene. Following the restriction digest, there should be two bands for the HA plasmid: one containing the HA tag at 300 bp (HA short) and a second containing the rest of the plasmid around 3,700 bp (HA long). There should be three bands for the FOXG1 plasmid, as there are two bbsI digestion sites: one containing the Myc tag around 300 bp (FOXG1 short), one containing the C-terminal region of FOXG1 around 40 bp, and the last containing the rest of the FOXG1 plasmid backbone around 6,000 bp (FOXG1 long). I did not expect to visualize the 40 bp band due to low molecular weight. I performed the restriction digests sequentially and verified the success of the reaction by running the product (Figure 3.13, lanes 1 and 2) on a gel alongside uncut plasmid (Figure 3.13, lanes 3 and 4). I cut out the bands using a UV light box and isolated the bands from the gel using a Wizard SV gel and PCR-clean up system (Promega, cat. no A9281).

Using T4 DNA ligase enzyme (New England BioLabs, cat no M0202S), I performed the reaction by combining the product HA short, FOXG1 long, and FOXG1 short (Figure 3.13, lanes 5-9). FOXG1 short was added because it contained the notI site necessary to complete the plasmid. I accompanied this with reactions that did not include the ligase or the inserts (HA or FOXG1 short) as controls (Figure 3.13, lanes 5-9). There was no size shift in the ligated product compared to the cut plasmid, suggesting the ligation reaction did not work.

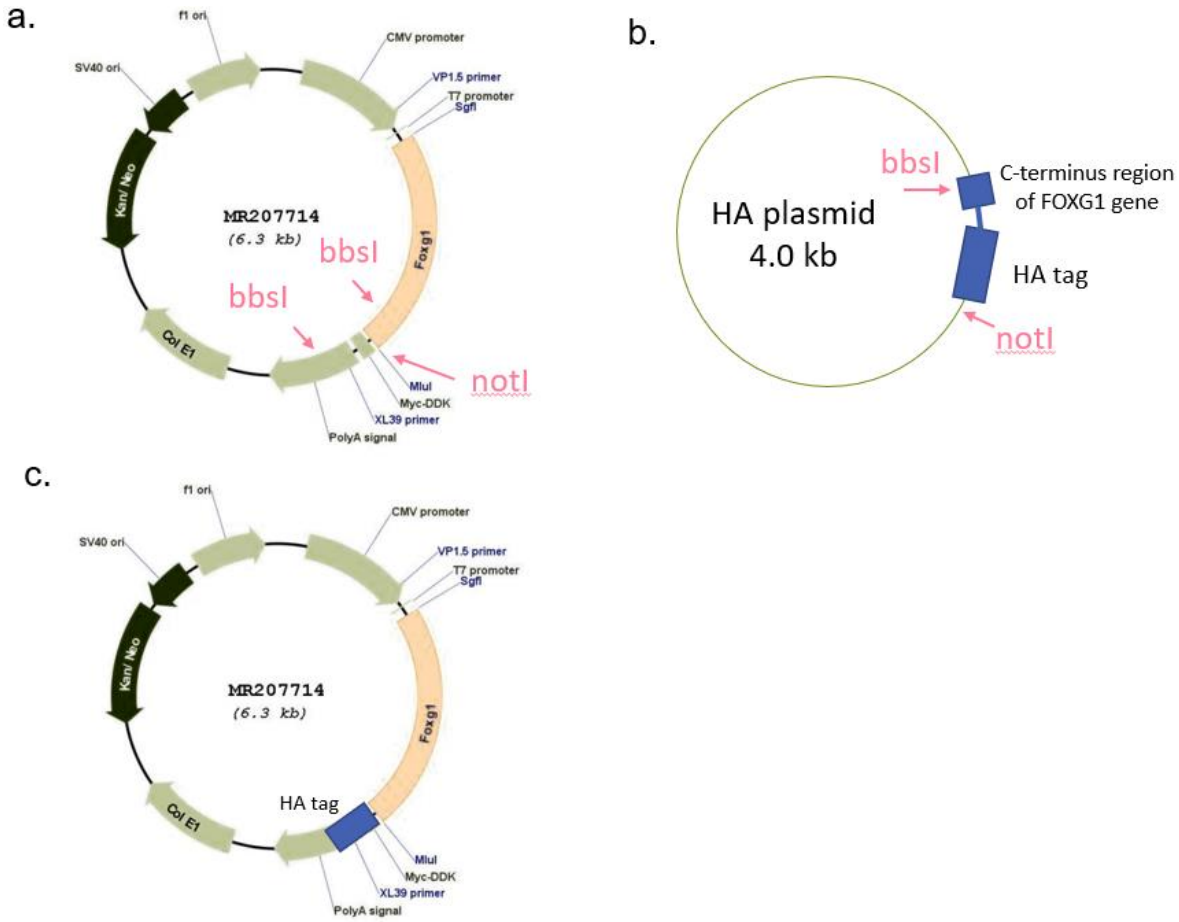

Figure 3.12. FOXG1 plasmid vector. **a**. Original plasmid from Origene with restriction sites. **b**. Structure of plasmid containing HA tag and C-terminal end of *FOXG1* gene. **c**. The expected structure of FOXG1-HA plasmid following ligation with the HA tag insert.

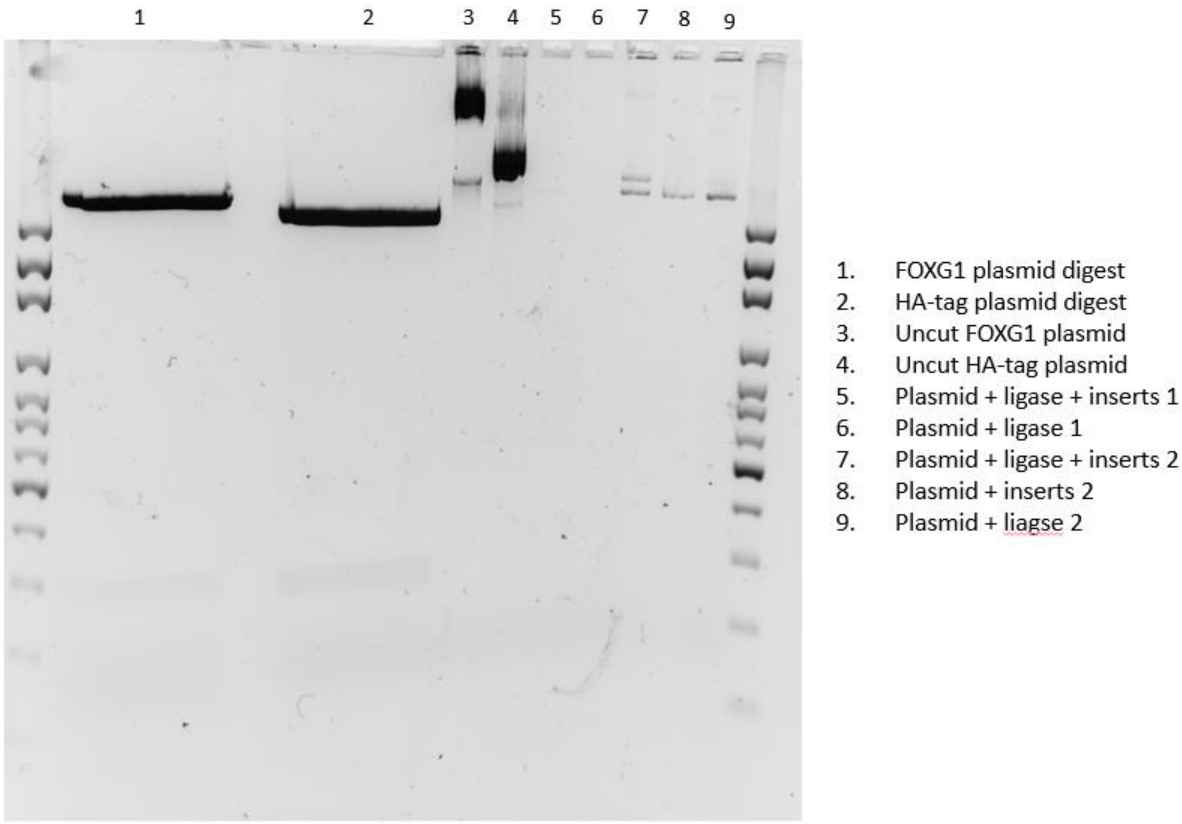

Figure 3.13. Image of agarose gel completed as part of the FOXG1-HA vector cloning project containing cut and uncut plasmids as well as ligation product.

Other observations

FOXG1-HA animals have been bred to maintain this mouse line. An observation I have made is that dams with the HA genotype do not raise their offspring unless a C57 foster mother has also been placed in the cage. This does not happen with KI dams. This leads me to believe that there is something about the FOXG1-HA protein that gives it a function that endogenous FOXG1 does not possess, and that is not caused by the presence of the SA/SC. There is also the possibility that the SA/SC are misplaced and are causing a mutation that interferes with the dams raising the offspring.

Discussion and Future Directions

Using the methods of western blotting, immunoprecipitation, and immunohistochemistry, the FOXG1-HA protein was not visualized. Sequencing the HA tag portion of the *FOXG1* gene, the HA tag was found to be present and in the correct place. There is yet more to be done to work towards confirming the presence of the FOXG1-HA protein. To start from the beginning, it needs to be verified in the mouse lines Nestin-Cre and HoxB1-Cre that Cre is being expressed in cortical tissues, since we genotype using tail snips and there is a possibility that recombination is not occurring in cortical tissues. Sequencing of the 5'UTR region from the genomic DNA of the FOXG1-HA gene to verify the successful recombination of the gene is yet to be completed, and there is a possibility that the stop cassette and splice acceptor sequences are incorrectly placed. Behavior as outlined in Chapter 2 should be run with FOXG1-HA animals to determine changes in phenotypes regardless of the verification of expression of FOXG1-HA protein.

To address the possibility of FOXG1-HA protein being unable to be expressed, being unstable once expressed, or folding incorrectly, the vector cloning would be beneficial to be completed, starting from both cDNA libraries as well as the plasmids already possessed. mRNA can be collected from FOXG1-HA embryos to address the potential of insufficient RNA yields,

as FOXG1 expression is highest in between embryonic day 13 and 17. It was also suggested that using the cDNA library method, a reaction containing 3% DMSO could uncurl the DNA.

Further protein work is also needed. I believe it would be beneficial to repeat the IP procedure with protein lysates from embryonic cortices. I believe it would also be apt to perform the IP procedure with the mouse anti HA.11 antibody as that antibody targets the specific sequence our HA tag is composed of. More IHC with the antigen retrieval protocol and mouse anti HA.11 would also be beneficial as further steps. To address the possibility of the presence of phosphorylated FOXG1 in the embryonic cortices, an IP with FOXG1 antibody followed a WB and probe for phospho-serine would be interesting.

REFERENCES

Ahlgren S, Vogt P and Bronner-Fraser M (2003). Excess FoxG1 Causes Overgrowth of the Neural Tube. *J Neurobiol*, **57**, 337-349.

Aimone JB, Wiles J, Gage FH (2006) Potential role for adult neurogenesis in the encoding of time in new memories. *Nat Neurosci,* **9**, 723–727.

Aizenman Y and Vellis J De (1987). Brain neurons develop in a serum and glial free environment: effects of transferrin, insulin, insulin-like growth factor-I and thyroid hormone on neuronal survival, growth and differentiation. *Brain Res*, **4**, 32-42.

Altman J, Das G (1965). Post-Natal Origin of Microneurones in the Rat Brain. *Nature*, **207**, 953-956.

Ariani F, Hayek G, Rondinella D, Artuso R… and Renieri A (2008). FOXG1 is Responsible for the Congenital Variant of Rett Syndrome. *Am J Hum Gen*, **83**, 89-93.

Avoli M, Curtis M De, Gnatkovsky V, Gotman J, Kohling R, Levesque M, Manseau F, Shiri Z and Williams S (2019). Specific imbalance of excitatory / inhibitory signaling establishes seizure onset pattern in temporal lobe epilepsy. *J Neurophysiol*, **115**, 3229-3237.

Baek ST, Copeland B, Yun E, Kwon S, Guiemez-Gamboa A, Schaffer A, Kim S, Kang H, Song S, Mather G and Gleeson J (2016). An AKT3-FOXG1-Reelin Network Underlies Defective Migration in Human Focal Malformations of Cortical Development. *Nat Med*, **21**, 1445-1454.

Brancaccio M, Pivetta C, Granzotto M, Filippis C and Mallamaci A (2010). Emx2 and Foxg1 inhibit gliogenesis and promote neuronogenesis. *Stem Cells*, **28**, 1206-1218.

Bredenkamp N, Seoighe C and Illing N (2007). Comparative evolutionary analysis of the FoxG1 transcription factor from diverse vertebrates identifies conserved recognition sites for microRNA regulation. *Dev Genes Evol*, **217**, 227-233.

Cargnin F, Kwon JS, Katzman S, Chen B, Lee JW and Lee SK (2018). FOXG1 Orchestrates Neocortical Organization and Cortico-Cortical Connections. *Neuron*, **100**, 1083-1096.e5.

Caronia-Brown G, Yoshida M, Gulden F, Assimacopoulos S and Grove EA (2014). The cortical hem regulates the size and patterning of neocortex. *Development*, **141**, 2855-2865.

Casanova MF, Buxhoeveden D and Gomez J (2003). Disruption in the Inhibitory Architecture of the Cell Minicolumn: Implications for Autism. *Prog Clin Neuro*, **9**, 496-507.

Chan D, Liu V, To R, Chiu P, Lee W, Yao K and Ngan H (2009). Overexpression of FOXG1 contributes to TGF-β resistance through inhibition of p21 WAF1/CIP1 expression in ovarian cancer. *Br J Cancer*, **101**,1433-1443.

Chen S-C, D'Arcangelo G, Curran T, Morgan J, Scares H and Miao G (2003). A protein related to extracellular matrix proteins deleted in the mouse mutant reeler. *Nature*, **374**, 719-723.

Chiola S, Do MD, Centrone L and Mallamaci A (2019). Foxg1 overexpression in neocortical pyramids stimulates dendrite elongation via hes1 and pCreb1 upregulation. *Cereb Cortex,* **29**, 1006-1019.

Colasante G, Lignani G and Rubio A (2015). Rapid Conversion of Fibroblasts into Functional Forebrain GABAergic Interneurons by Direct Genetic Reprogramming. *Cell Stem Cell*, **17**, 719-734.

Dastidar S, Landrieu P and D'Mello S (2011). FoxG1 Promotes the Survival of Postmitotic Neurons. *J Neurosci*, **31**, 402-413.

Dastidar SG, Bardai FH, Ma C, Price V, Rawat V, Verma P, Narayanan V and D'Mello S (2012). Isoform-Specific Toxicity of Mecp2 in Postmitotic Neurons: Suppression of Neurotoxicity by FoxG1. *J Neurosci*, **32**, 2846-2855.

Dou C, Lee J, Liu B, Liu F, Massague J, Xuan S and Lai E (2000). BF-1 Interferes with Transforming Growth Factor beta Signaling by Associating with Smad Partners. *Mol Cell Biol*, **20**, 6201-6211.

Derynck R and Zhang YE (2003). Smad-dependent and Smad-independent pathways in TGF-β. *Nature*, **425**, 577-584.

Duggan C, DeMaria S, Baudhuin A, Stafford D and Ngai J (2008). Foxg1 is Required for Development of the Vertebrate Olfactory System. *J Neurosci*, **28**, 5229-5239.

Eiraku M, Watanabe K, Matsuo-Takasaki M, Kawada M, Yonemura S, Matsumura M, Wataya T, Nishiyama A, Muguruma K and Sasai Y (2008). Self-Organized Formation of Polarized Cortical Tissues from ESCs and Its Active Manipulation by Extrinsic Signals. *Cell Stem Cell*, **3**, 519-532.

Falcone C, Santo M, Liuzzi G, Cannizzaro N, Grudina C, Valencic E, Peruzzotti-Jametti L, Pluchino S and Mallamaci A (2019). *Foxg1* Antagonizes Neocortical Stem Cell Progression to Astrogenesis. *Cereb Cortex*, 1-16.

Gioran A, Nicotera P and Bano D (2014). Impaired mitochondrial respiration promotes dendritic branching via the AMPK signaling pathway. *Cell Death Dis*, **5**, e1175-8.

Guy J, Gan J, Selfridge J, Cobb S and Bird A (2007). Reversal of Neurological Defects in a Mouse Model of Rett Syndrome. *Science*, **315**, 1143-1147.

Han X, Gu X, Zhang Q, Wang Q, Cheng Y, Pleasure S and Zhao C (2018). FoxG1 Directly Represses Dentate Granule Cell Fate During Forebrain Development. *Front Cell Neurosci*, **12**, 1-13.

Hanashima C, Li S, Shen L, Lai E and Fishell G (2004). Foxg1 Suppresses Early Cortical Cell Fate. *Science*, **303**, 56-59.

Hanashima C, Shen L, Li S and Lai E (2002). Brain Factor-1 Controls the Proliferation and Differentiation of Neorcortical Progenitor Cells Through Independent Mechanisms. *J Neurosci*, **22**, 6526-6536.

Hatini V, Ye X, Balas G and Lai E (1999). Dynamics of placodal lineage development revealed by targeted transgene expression. *Dev Dyn*, **215**, 332-343.

Kumamoto T, Toma K, Gunadi, McKenna W, Kasukawa T, Katzman S, Chen B and Hanashima C (2013). Foxg1 Coordinates the Switch from Non-Radioally to Radially Migrating Glutamatergic Subtypes in the Neocortex through Spatiotemporal Regulation. *Cell Rep*, **3**, 931-945.

Latchman DS (1997). Transcription Factors: An Overview. *Int J Biochem Cell Biol*, **29**, 1305-1312.

Lehmann OJ, Sowden JC, Carlsson P, Jordan T and Bhattacharya SS (2003). Fox's in development and disease. *Trends Genet*, **19**, 339-344.

Li J, Chang HW, Lai E, Parker E and Vogt P (1995). The Oncogene qin Codes for a Transcriptional Repressor. *Cancer Res*, **55**, 5540-5545.

Liu B, Zhou K, Wu X and Zhao C (2018). Foxg1 deletion impairs the development of the epithalamus. *Mol Brain*, **11**, 1-11.

Mambetisaeva ET, Andrews W, Camurri L, Annan A and Sundaresan V (2005). Robo family of proteins exhibit differential expression in mouse spinal cord and robo-slit interaction is required for midline crossing in vertebrate spinal cord. *Dev Dyn*, **233**, 41-51.

Marcal N, Patel H, Dong Z, Belanger-Jasmin S, Hoffman B, Dang J and Stifani S (2005). Antagonistic effects of Grg6 and Groucho/TLE on the transcription repression activity of brain factor 1/FoxG1 and cortical neuron differentiation. *Mol Cell Biol*, **25**, 10916-29.

Mariani J, Coppola G, Zhang P, Abyzov A, Provini L, Tomasini L, Amenduni M, Szekely A, … Vaccarino F (2015). FOXG1-dependent Dysregulation of GABA/glutamate Neuron Differentiation in Autism Spectrum Disorder. *Cell*, **162**, 375-390.

Martynoga B, Morrison H, Price DJ and Mason JO (2005). Foxg1 is required for specification of ventral telencephalon and region-specific regulation of dorsal telencephalic precursor proliferation and apoptosis. *Dev Biol*, **283**, 113-127.

Mattson M, Gleichmann M and Cheng A (2008). Mitochondria in Neuroplasticity and Neurological Disorders. *Neuron*, **60**, 748-766.

Mitter D, Pringsheim M, Kaulisch M, et al (2018). FOXG1 syndrome: Genotype-phenotype association in 83 patients with FOXG1 variants. *Genet Med*, **20**, 98-108.

Murphy D, Wiese S and Burfeind P (1994). Human Brain Factor 1, a New Member of the Fork Head Gene Family. *Genomics*, **21**, 551-557.

Regad T, Roth M, Bredenkamp N, Illing N and Papalopulu N (2007). The neural progenitor-specifying activity of FoxG1 is antagonistically regulated by CKI and FGF. *Nat Cell Biol*, **9**, 531-540.

Pancrazi L, Di Benedetto G, Colombaioni L, Sala G, Testa G, Olimpico F, Reyes A, Zeviani M, Pozzan T and Costa M (2015). Foxg1 localizes to mitochondria and coordinates cell differentiation and bioenergetics. *Proc Natl Acad Sci*, **112**, 13910-13915.

Patriarchi T, Amabile S, Frullanti E, Landucci E, Rizzo C, Ariani F, Costa M, Olimpico F, Hell J, Vaccarino F, Renieri A, Meloni I (2016). Imbalance of excitatory/inhibitory synaptic protein expression in iPSC-derived neurons from FOXG1 patients and in foxg1 mice. *Eur J Hum Genet*, **24**, 871-880.

Pauley S, Lai E and Fritzsch B (2006). Foxg1 is required for morphogenesis and histogenesis of the mammalian inner ear. *Dev Dyn*, **235**, 2470-2482.

Pelton RW, Saxena B, Jones M, Moses HL and Leslie I (1991). Immunohistochemical Localization of TGFβ1, TGFβ2, and TGFβ3 in the Mouse Embryo: Expression Patterns Suggest Multiple Roles during Embryonic Development. *Cell Bio*, **115**, 1091-1105.

Polleux F, Dehay C and Kennedy H (1997). The timetable of laminar neurogenesis contributes to the specification of cortical areas in mouse isocortex. *J Comp Neurol*, ***385***, 95-116.

Pratt T, Quinn JC, Simpson TI, West JD, Mason JO and Price DJ (2002). Disruption of early events in thalamocortical tract formation in mice lacking the transcription factors Pax6 or Foxg1. *J Neurosci*, **22**, 8523-8531.

Renner M, Lancaster MA, Bian S, Choi H, Ku T, Peer A, Chung K and Knoblich J (2017). Self-organized developmental patterning and differentiation in cerebral organoids. *Embo J*, **36**, 1316-1329.

Roesch A, Mueller AM, Stempfl T, Moehle C, Landthaler M and Vogt T (2008). RBP2-H1/JARID1B is a transcriptional regulator with a tumor suppressive potential in melanoma cells. *Int J Cancer*, **122**, 1047-1057.

Rubenstein JLR (2010). Three hypotheses for developmental defects that may underlie some forms of autism spectrum disorder. *Curr Opin Neurol*, **23**, 118-123.

Shibata M, Kurokawa D, Nakao H, Ohmura T and Aizawa S (2008). MicroRNA-9 Modulates Cajal – Retzius Cell Differentiation by Suppressing Foxg1 Expression in Mouse Medial Pallium. *J Neurosci*, **28**, 10415-10421.

Siegenthaler JA and Miller MW (2005). Transforming Growth Factor β1 Promotes Cell Cycle Exit through the Cyclin-Dependent Kinase Inhibitor p21 in the Developing Cerebral Cortex. *J Neurosci*, **25**, 8627-8636.

Siegenthaler JA, Tremper-Wells BA and Miller MW (2008). Foxg1 haploinsufficiency reduces the population of cortical intermediate progenitor cells: effect of increased p21 expression. *Cereb Cortex*, **18**, 1865-1875.

Sztainberg Y, Chen H, Swann JW, Hao S, Tang B, Wu Z, Tang J, Wan Y, Liu Z, Rigo F and Zoghbi H (2016). Reversal of Phenotypes in MECP2 Duplication Mice Using Genetic Rescue or Antisense Oligos. *Nature*, **528**, 123-126.

Tao W and Lai E (1992). Telencephalon-restricted expression of BF-1, a new member of the HNF-3/fork head gene family, in the developing rat brain. *Neuron*, **8**, 957-966.

Testa G, Mainardi M, Olimpico F, Pancrazi L, Caleo M and Costa M (2019). A triheptanoin-supplemented diet rescues hippocampal hyperexcitability and seizure susceptibility in FoxG1+/− mice. *Neuropharmacology*, **148**, 305-310.

Tian C, Gong Y, Yang Y, Shen W, Wang K, Liu J, Xu B, Zhao J and Zhao C (2012). Foxg1 Has an Essential Role in Postnatal Development of the Dentate Gyrus. *J Neurosci*, **32**, 2931-2949.

Vegas N, Cavallin M, Maillard C and Boddaert N (2018). Delineating FOXG1 syndrome - From congenital microcephaly to hyperkinetic encephalopathy. *Neurol Genet*, **4**, e281.

Verginelli F, Perin A, Dali R, Fung K and Lo R (2013). Transcription factors FOXG1 and Groucho/TLE promote glioblastoma growth. *Nat Commun*, **4**, 2956.

Vezzali R, Weise SC, Hellbach N, Machado V, Heidrich S and Vogel T (2016). The FOXG1/FOXO/SMAD network balances proliferation and differentiation of cortical progenitors and activates Kcnh3 expression in mature neurons. *Oncotarget*, **7**, 37436-37455.

Yang Y, Shen W, Ni Y, Su Y, Yang Z and Zhao C (2017). Impaired Interneuron Development after Foxg1 Disruption. *Cereb Cortex*, **27**, 793-808.

Zhang X, Bertaso F, Yoo JW, Baumgärtel K, Clancy SM, Lee V, Cienfuegos C, Wilmot C, Avis J, Hunyh T, Daguia C, Schmedt C, Noebels J and Jegla T (2010). Deletion of the potassium channel Kv12.2 causes hippocampal hyperexcitability and epilepsy. *Nat Neurosci*, **13**, 1056–8.